

Precipitation extremes over the continental United States in a transient, high-resolution, ensemble climate model experiment

Deepti Singh,¹ Michael Tsiang,¹ Bala Rajaratnam,^{1,2} and Noah S. Diffenbaugh^{1,3,4}

Received 25 December 2012; revised 31 May 2013; accepted 31 May 2013; published 11 July 2013.

[1] Understanding future changes in the frequency, intensity, and duration of extreme events in response to increased greenhouse gas forcing is important for formulating adaptation and mitigation strategies that minimize damages to natural and human systems. We quantify transient changes in daily-scale seasonal extreme precipitation events over the U.S. using a five-member ensemble of nested, high-resolution climate model simulations covering the 21st century in the Intergovernmental Panel on Climate Change (IPCC) Special Report on Emission Scenarios (SRES) A1B scenario. We find a strong drying trend in annual and seasonal precipitation over the Southwest in autumn, winter, and spring and over the central U.S. in summer. These changes are accompanied by statistically significant increases in dry-day frequency and dry-spell lengths. Our results also show substantial increases in the frequency of extreme wet events over the northwestern U.S. in autumn, winter, and spring and the eastern U.S. in spring and summer. In addition, the average precipitation intensity increases relative to the extreme precipitation intensity in all seasons and most regions, with the exception of the Southeast. Further, most regions receive a greater fraction of total seasonal precipitation from extreme events. These results imply fewer but heavier precipitation events in the future, leading to more frequent wet and dry extremes in most regions of the U.S. Our simulations suggest that many of these changes are likely to become statistically significant by the mid-21st century. Given current vulnerabilities, such changes in extreme precipitation could be expected to increase stress on water resources in many areas of the U.S., including during the near-term decades.

Citation: Singh, D., M. Tsiang, B. Rajaratnam, and N. S. Diffenbaugh (2013), Precipitation extremes over the continental United States in a transient, high-resolution, ensemble climate model experiment, *J. Geophys. Res. Atmos.*, 118, 7063–7086, doi:10.1002/jgrd.50543.

1. Introduction

[2] In 2011 alone, the U.S. experienced a record number of weather and climate extremes, of which 14 events caused damages exceeding \$1 billion dollars each, including the loss of lives [Lott *et al.*, 2012]. Almost every state in the contiguous U.S. experienced wet or dry extremes in 2011 and 2012 [NOAA, 2011, 2012a, 2012b]. Approximately 9% of the U.S. experienced a severely wet 2011–2012 winter season [NOAA, 2012a], and over 60% was under moderate to severe drought by the end of summer 2012 [NOAA, 2012b].

Additional supporting information may be found in the online version of this article.

¹Department of Environmental Earth System Science, Stanford University, Stanford, California, USA.

²Department of Statistics, Stanford University, Stanford, California, USA.

³Woods Institute for the Environment, Stanford University, Stanford, California, USA.

⁴Department of Earth and Atmospheric Sciences and Purdue Climate Change Research Center, Purdue University, West Lafayette, Indiana, USA.

Corresponding author: D. Singh, Department of Environmental Earth System Science, Stanford University, 473 Via Ortega, Jerry Yang and Akiko Yamazaki Environment and Energy Building, Stanford, CA 94305-4216, USA. (singhd@stanford.edu)

©2013. American Geophysical Union. All Rights Reserved.
2169-897X/13/10.1002/jgrd.50543

[3] These severe conditions over much of the U.S. in 2011 and 2012 have occurred within the context of a changing hydroclimatic regime. The hydroclimatic intensity has increased over the U.S. as a whole in recent decades [Giorgi *et al.*, 2011], along with positive trends in the frequency and intensity of heavy precipitation events over parts of the U.S. [Pryor *et al.*, 2009; Gleason *et al.*, 2008; Peterson *et al.*, 2008]. Significant positive trends detected in mean precipitation and in the atmospheric moisture content have been formally attributed to anthropogenic emissions of greenhouse gases [Zhang *et al.*, 2007; Santer *et al.*, 2007]. Recent studies have found significant changes in the frequency and intensity of wet and dry extremes in some regions, along with an expansion of the areas experiencing extremes [Mishra and Lettenmaier, 2011; Field *et al.*, 2012; Easterling, 2000; Allen and Ingram, 2002; Zhang *et al.*, 2007; Allan and Soden, 2008; Burke *et al.*, 2006; Lintner *et al.*, 2012]. Further, the Intergovernmental Panel on Climate Change (IPCC) Special Report on Extremes suggests that increasing anthropogenic greenhouse gases are likely to cause more intense and longer droughts [Field *et al.*, 2012].

[4] As has been observed in recent years in the U.S., hydroclimatic extremes such as heavy precipitation events and long dry periods can result in severe damage to human

systems through direct and indirect impacts on water supply, agriculture, and energy infrastructure (such as dams and power plant cooling) [Kunkel et al., 1999; Rosenzweig et al., 2001; Rosenzweig et al., 2002]. Therefore, understanding possible future changes in the occurrence of precipitation extremes can minimize catastrophic losses to life and property and lessen economic damages through suitable adaptation and mitigation strategies.

[5] Future global warming is likely to affect the hydrological cycle through changes in the atmospheric moisture content, saturation vapor pressure, evapotranspiration, and horizontal and vertical mass transport [Held and Soden, 2006; Allen and Ingram, 2002; O'Gorman and Schneider, 2009]. In general, enhancement of the hydrological cycle is expected to cause many wet regions to become wetter and many dry regions to become drier [Held and Soden, 2006; Tebaldi et al., 2006; Lintner et al., 2012]. However, mean and extreme precipitation changes are nonlinearly related on both a seasonal and annual scale [Wehner, 2004], and extremes tend to increase at a faster rate relative to mean precipitation in the subtropics and over most of North America [Emori and Brown, 2005; Russo and Sterl, 2012]. The atmospheric water vapor content increases with atmospheric temperature at an approximate rate of 7.5% per kelvin, in accordance with the Clausius-Clayperon relationship [Held and Soden, 2006; Trenberth et al., 2003; Wentz et al., 2007]. Precipitation extremes are more sensitive to increases in atmospheric moisture content relative to mean precipitation [Trenberth, 1999; Allen and Ingram, 2002; O'Gorman and Schneider, 2009; Emori and Brown, 2005; Allan and Soden, 2008; Katz and Brown, 1992]. Their response to global warming is also proportional to changes in temperature and net vertical velocity that influence the moist-adiabatic lapse rate [O'Gorman and Schneider, 2009; Emori and Brown, 2005]. As a consequence of these thermodynamic and dynamic control factors, the response of precipitation extremes to global warming is likely to be different in different seasons of the annual cycle [Emori and Brown, 2005; Wehner, 2004; Noake et al., 2012].

[6] General circulation model (GCM) experiments indicate that future warming is likely to affect many metrics of precipitation extremes [Meehl et al., 2006; Diffenbaugh and Ashfaq, 2010; Tebaldi et al., 2006; Giorgi et al., 2011]. Analyses of 21st century CMIP3 model projections suggest that precipitation events greater than 10 mm, the 5 day total precipitation, precipitation events exceeding the 95th percentile, and the average precipitation intensity are all likely to increase in response to global warming [Tebaldi et al., 2006]. Burke et al. [2006] project less frequent but longer dry spells at the end of the 21st century under the A2 Special Report on Emission Scenarios (SRES) with a substantial increase in the global land area experiencing extreme drought (from 1–3% presently to approximately 30%). Further, North America is likely to experience consistent positive trends in extreme precipitation events with increased warming [Field et al., 2012] and higher hydroclimatic intensity, a result of increases in both precipitation intensity and dry-spell lengths [Giorgi et al., 2011]. Studies suggest substantial changes in interannual precipitation variability over the northwestern U.S., southern California, Mexico, and Texas [Diffenbaugh et al., 2008] and increases in the frequency and contribution of extreme precipitation events over coastal regions in the eastern U.S.

and rain-shadow regions in the western U.S. and Canada [Diffenbaugh et al., 2005]. Further, Dominguez et al. [2012] project robust increases in the intensity of winter precipitation extremes over the western U.S. toward the latter half of the 21st century [Dominguez et al., 2012].

[7] In the present study, we seek to understand the transient changes in extreme precipitation over the continental U.S. under the A1B SRES scenario. We use a multi-ensemble, high-resolution, transient climate model experiment [Diffenbaugh et al., 2011; Diffenbaugh and Ashfaq, 2010] to simulate the processes influencing the frequency, intensity, and duration of extremes. Although much has been learned from the analysis of relatively low-resolution GCMs, high-resolution climate models that resolve topographical features and capture fine-scale climate processes such as surface moisture and snow albedo feedbacks [Diffenbaugh et al., 2005; Diffenbaugh et al., 2011; Dominguez et al., 2012] can more accurately simulate observed precipitation extremes [Duffy et al., 2003; Walker and Diffenbaugh, 2009]. In addition to resolving the present climate, these physical factors are also important in regulating the response of precipitation extremes to increasing greenhouse forcing [O'Gorman and Schneider, 2009; Diffenbaugh et al., 2005]. Likewise, multi-member climate model experiments can simulate the internal variability of the climate system that is particularly important in the near-term trajectory of regional precipitation [Hawkins and Sutton, 2009, 2011]. Further, continuous, multi-decadal experiments provide the ability to examine the timing and magnitude of the changes in response to transient changes in radiative forcing [Hawkins and Sutton, 2009, 2011; Christensen et al., 2007; Diffenbaugh et al., 2011]. Because natural and human systems are adapted to the variability of the current climate, the timing of emergence of changes above the present climate variability (noise) is critical for both adaptation planning and for setting mitigation targets that are likely to influence future emission trends [Diffenbaugh et al., 2011; Hawkins and Sutton, 2011].

[8] Most previous studies examining changes in regional extreme precipitation in response to increased greenhouse gas forcing use smaller nested domains, shorter simulation periods, and single realizations of a given model [Dominguez et al., 2012; Diffenbaugh et al., 2005]. However, analyzing the time-varying signal-to-noise ratio is only possible with a transient, multi-member experiment. The multi-member ensemble we analyze is unprecedented in its temporal extent (1950–2099) at a spatial coverage that includes the entire continental U.S. in the high-resolution, nested domain. Using continuous, daily data from this ensemble, we present the first analysis of the transient response of daily-scale extreme precipitation to transient increases in greenhouse gas concentrations.

2. Methods

2.1. Climate Model Experiments

[9] We analyze daily precipitation data from a transient, physically uniform, high-resolution, multi-member ensemble climate model experiment over the continental United States [Diffenbaugh et al., 2011; Diffenbaugh and Ashfaq, 2010]. The experiment spans the period from 1950 to 2099, with the 20th century forced by observed atmospheric constituent concentrations and the 21st century period forced by the Special Report on Emission Scenarios (SRES) A1B scenario [Nakicenovic et al., 2000]. The

SRES A1B is a medium-forcing scenario with atmospheric CO₂ concentrations increasing to 700 ppm by the end of the 21st century. The simulations are performed using the Abdus Salam International Center for Theoretical Physics high-resolution, hydrostatic nested climate model (RegCM3). The equal-area grid follows *Diffenbaugh et al.* [2005] and has a 25 km horizontal resolution and 18 vertical levels. (To avoid the inclusion of discontinuities at the boundary of the nested domain, eight grid points are discarded from each side.) *Pal et al.* [2007] describe the physical parameterizations of RegCM3, while *Diffenbaugh et al.* [2011] provide more details of the experiment.

[10] Large-scale boundary conditions for the nested RegCM3 are provided by the National Center for Atmospheric Research (NCAR) Community Climate System Model version 3 (CCSM3) atmosphere-ocean GCM. One RegCM3 realization is nested within each of five CCSM3 realizations (identified by NCAR as c, e, bES, fES, and gES). These five CCSM3 realizations are described in *Meehl et al.* [2006] and included in NCAR's contribution to the CMIP3 archive [*Meehl et al.*, 2007]. The five CCSM3 realizations are initialized at different points in the same preindustrial simulation and are given identical radiative forcings for the historical and future time periods.

[11] Like the five CCSM3 realizations, the five RegCM3 realizations have identical model configurations and receive identical time series of atmospheric constituents over the course of the transient experiment. The RegCM3 (referred to further as CCSM3-RegCM3 ensemble) simulations, therefore, form a physically uniform high-resolution ensemble. The only difference between the five RegCM3 realizations is the time series of sea surface temperatures (SSTs), sea ice, and atmospheric lateral boundary conditions that each RegCM3 realization receives from the CCSM3 realization in which it is nested. These differences in SSTs, sea ice, and atmospheric lateral boundary conditions result from internal climate system variability simulated by the CCSM3 atmosphere-ocean GCM. The RegCM3 simulations are initialized in 1950, while our analysis begins in 1970, allowing two complete decades for model equilibration.

[12] In addition, we use the multi-model ensemble of nested, high-resolution simulations that is part of the North American Regional Climate Change Assessment Program (NARCCAP) project [*Mearns et al.*, 2009; *Mearns et al.*, 2007; *Mearns et al.*, 2012] for comparison of the present simulations. The ensemble is generated from six regional climate models (RCM) nested within four different atmosphere-ocean general circulation models (AOGCM) at a 50 km horizontal resolution. CCSM3 is one of the four driving AOGCMs, and RegCM3 is one of the six nested RCMs. Further, the simulation domain of the NARCCAP ensemble members includes the continental U.S. and most of Canada. Simulations are run for 30 years in the late twentieth century (1971–2000) and mid-21st century (2041–2070) under the SRES A2 emission scenario [*Nakicenovic et al.*, 2000] and archived every 3 hours. We exclude the last year of each simulation period from our comparative analysis because of the unavailability of complete data for some of the members. These climate models differ in their formulation of the physics and parameterization schemes. Consequently, the ensemble provides an opportunity to compare the spread resulting from model differences with the intra-ensemble spread

obtained from the CCSM3-RegCM3 ensemble, even though the NARCCAP simulations are at a lower resolution.

2.2. Observations

[13] We use daily precipitation from the National Oceanic and Atmospheric Administration (NOAA) Climate Prediction Center (CPC) $0.25^\circ \times 0.25^\circ$ US Unified data set [*Higgins et al.*, 2000] as the reference for validation of our simulations. High-resolution gridded data are available for the continental U.S. (approximately 20°N – 60°N and 140°W – 60°W) for the period from 1948 to 2006.

2.3. Metrics and Statistics

[14] In the following analyses, we define our 30 year baseline period from 1970 to 1999. We examine the transient response of precipitation extremes to warming on annual and seasonal time scales over the near-term (2010–2039), medium-term (2040–2069) and long-term (2070–2099) periods. Following *Salinger and Griffiths* [2001], we define dry days and rain days as days with precipitation below and above the 1 mm/day threshold, respectively.

[15] The extreme precipitation metrics follow those of *Diffenbaugh et al.* [2005], *Walker and Diffenbaugh* [2009], *Frich et al.* [2002], and *Giorgi et al.* [2011]. We define wet extremes based on the average baseline 95th percentile of daily precipitation (P95) at each grid point. The baseline P95 value at each grid point is an average of the 95th percentile daily precipitation magnitude of rain days in each year of the baseline period. We then calculate the number of days exceeding this P95 value at each grid point during each year of the baseline and future periods as a measure of wet extremes. We express the extreme precipitation fraction as a ratio of precipitation from wet extreme events to the total precipitation. The average precipitation intensity refers to the ratio of total precipitation to the total number of rain days. We similarly determine the intensities of extreme events and non-extreme events (rain days with precipitation below the P95 value). Further, we calculate the dry spell and wet spell lengths as the number of consecutive dry days or wet extremes respectively, at each grid point.

[16] In this study, we define the seasons as December–January–February (winter), March–April–May (spring), June–July–August (summer), and September–October–November (autumn). For the annual timescale, we calculate the metrics using all days during the year. For the seasonal analysis, we define our metrics using the days within each season of every year. As an example, in the analysis of winter wet extremes, we average the 95th percentile daily winter precipitation value from each of the 30 years of the baseline (1970–1999). We then find the number of days exceeding that baseline winter P95 value in all winter seasons of each period in the 21st century. Similarly, we define the remaining extreme precipitation metrics based on these respective seasonal 95th percentile values.

[17] Figure 1 shows the U.S. regions as defined for the National Climate Assessment (NCA) [*NAST*, 2000], over which some extreme precipitation metrics are analyzed. In quantifying the regional changes in the extreme precipitation metrics, we first calculate the extreme precipitation metrics at each grid point within a NCA region for each decade and average the calculated metric across all ensemble members. We then average the metrics from all grid points within a

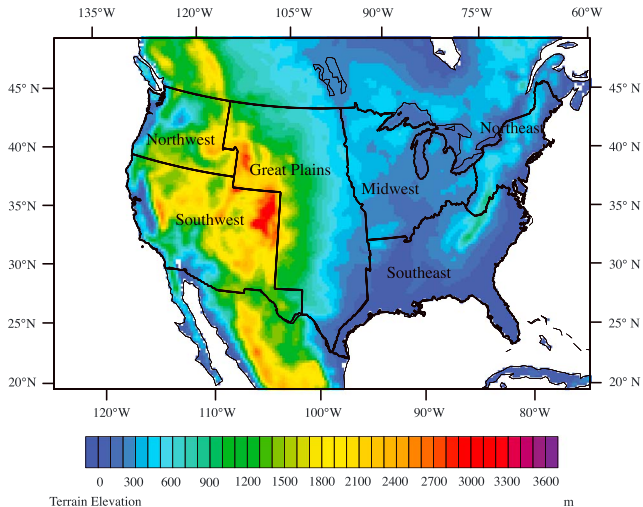


Figure 1. Topographical map of the contiguous United States showing the regions defined for the National Climate Assessment [NAST, 2000].

region to define its regional average value and calculate changes in these values in the future 30 year time periods relative to the baseline.

[18] Relative changes in the metrics at each spatial point are calculated from ensemble-average values in the 30 year periods of the baseline and the 21st century. We apply the binomial test for testing the significance of the difference in proportions of wet extreme events between any 21st century period and the baseline. The null hypothesis for the binomial test is that the proportions of wet extremes in both time periods equal 0.05 (based on our definition of wet extremes). Figure S1 in the supporting information shows the distributions of each metric at six spatial points, one from each of the six NCA regions, and the p values from the Anderson-Darling test for normality of the distributions. Since the assumption of normality does not consistently hold true, we use the two-tailed, nonparametric Mann-Whitney U test to examine the statistical significance of simulated changes in all other metrics. We aggregate data from all five-ensemble members, providing 150 samples in each time period for significance testing. Regions experiencing statistically significant changes at the 5% level are shown by stippling on the maps (such as in Figure 4). Since 5% of these tests are significant by chance under the null hypothesis, we exclude 5% of points with the lowest p values from the set of spatial points that are classified as statistically significant. The set of excluded spatial points for each metric are shown in Figure S2.

2.4. Model Evaluation

[19] A primary motivation for high-resolution climate modeling is to improve the resolution of the fine-scale climate processes that can regulate climate extremes [Diffenbaugh et al., 2005; Di Luca et al., 2012; Diffenbaugh and Ashfaq, 2010; Duffy et al., 2003]. RegCM3 has been used extensively to study the climate dynamics of various regions of the world, driven by several GCMs [Ashfaq et al., 2010; Lionello and Giorgi, 2007; Gao and Giorgi, 2008; Ballester et al., 2010; Seth et al., 2007; Diffenbaugh et al., 2005; Rauscher et al., 2008] including CCSM3 [Diffenbaugh and Ashfaq, 2007; Ashfaq et al., 2009; Trapp et al., 2009; Diffenbaugh et al.,

2011]. Studies over the contiguous United States, including those that analyze results from the multi-model NARCCAP ensemble, suggest that RegCM3 can capture the observed spatial patterns of temperature and precipitation, atmospheric circulation patterns, evapotranspiration, and snowmelt-driven surface runoff in the historic period [Walker and Diffenbaugh, 2009; Wang et al., 2009; Gutowski et al., 2010; Rauscher et al., 2008]. National Center for Climate Prediction (NCEP)-Department of Energy (DOE) global reanalysis data (R2) [Kanamitsu et al., 2002] provides boundary conditions for RegCM3 in most of these evaluation studies [Walker and Diffenbaugh, 2009; Wang et al., 2009; Gutowski et al., 2010]. The model also captures the seasonal and interannual variability of temperature and precipitation [Walker and Diffenbaugh, 2009; Gutowski et al., 2010]. Additionally, RegCM3 simulates the environmental conditions associated with severe thunderstorms over the central U.S. [Trapp et al., 2007a]. However, although the model simulates the basic structure of the surface winds [Walker and Diffenbaugh, 2009; Diffenbaugh and Ashfaq, 2007], the model underestimates the interannual wind variability and does not fully capture the spatial variations of surface winds [Pryor and Barthelmie, 2011; Rasmussen et al., 2011]. At the 25 km resolution, the mean seasonal temperature and precipitation patterns are closely captured even though some biases still exist due to anomalous winds, soil moisture, and heat fluxes in some seasons and regions [Walker and Diffenbaugh, 2009; Diffenbaugh and Ashfaq, 2010; Ashfaq et al., 2010].

[20] The emphasis of the current study is on the response of precipitation extremes to elevated greenhouse forcing. Our metrics build on those of Walker and Diffenbaugh [Walker and Diffenbaugh, 2009], who evaluate NCEP-DOE R2 driven RegCM3 simulation of precipitation extremes in the historic period. Walker and Diffenbaugh [2009] show that RegCM3 can simulate the observed mean and interannual variability of daily-scale extreme temperature and precipitation events over most parts of the continental U.S. In particular, the complex topography of the Cascades and Sierra Nevada ranges is represented in the high-resolution RegCM3, and the model captures the peak precipitation in the Intermountain Regions. However, some biases exist in simulating extreme precipitation over the topographically complex regions [Wang et al., 2009; Walker and Diffenbaugh, 2009], with excess extreme precipitation over high elevations being attributed to excessively strong winds in RegCM3 [Walker and Diffenbaugh, 2009].

[21] We evaluate the performance of the CCSM3-RegCM3 and NARCCAP ensembles in capturing the observed spatial patterns of annual extreme precipitation metrics for the baseline period (1970–1999) (Figure 2). The CCSM3-RegCM3 ensemble overestimates mean annual precipitation, wet extreme days, and number of rain days over the mountainous regions in western U.S., the Northeast, and the northern Great Plains and precipitation intensities in the Central Valley (Figure S3). In addition, it underestimates these variables over the Southeast and parts of central U.S. The CCSM3-RegCM3 ensemble accurately simulates the observed spatial patterns of most metrics with the exception of the extreme precipitation fraction (Figure 2). The spatial correlations for these metrics (except extreme precipitation fraction) exceed 0.6. However, the ensemble demonstrates greater spatial variability of wet extremes and dry days and

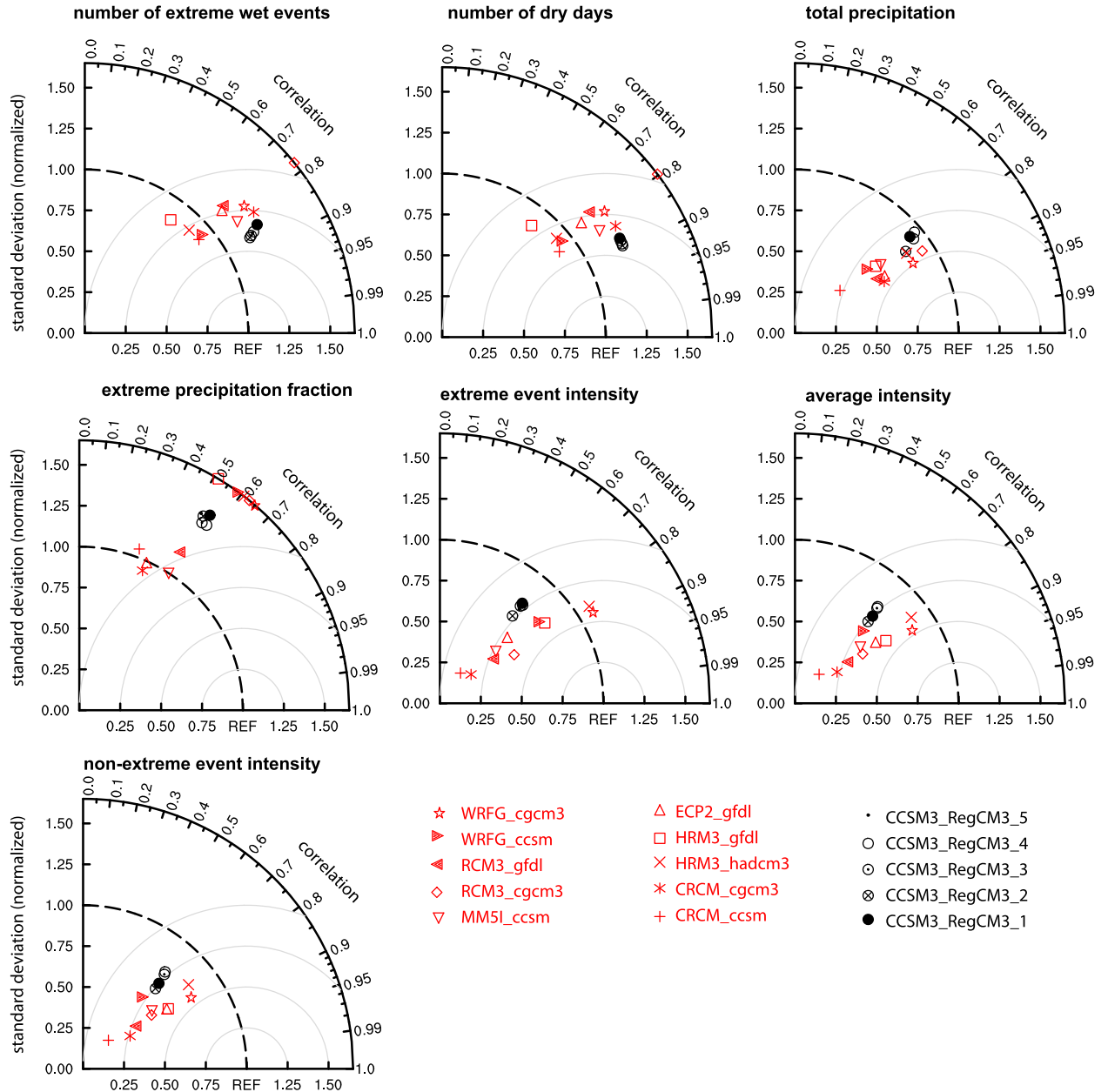


Figure 2. Taylor diagram to compare the skill of the CCSM3-RegCM3 and NARCCAP ensembles in representing the annual extreme precipitation characteristics over the continental U.S., using the NOAA CPC precipitation observations as reference. Evaluation based on the baseline period (1970–1999). Symbols represent models (red, NARCCAP; black, CCSM3-RegCM3), and each panel represents a metric. Position in the azimuthal direction represents the pattern spatial correlation. Location in the radial direction represents the spatial variability normalized by the observed variability of the metric. Distance from the reference (REF) point provides the normalized RMS error between the simulations and observations (gray contours represent RMS errors of the metric). Models closest to the reference location best represent the observed spatial pattern of the metric.

lower spatial variability of precipitation intensities over the U.S. Further, there is little spread in the spatial correlation, root mean square error (RMSE), and spatial variability of the five ensemble members. In contrast, there is considerable spread amongst the 10 NARCCAP ensemble members in simulating the spatial patterns of the observed precipitation metrics. The RMSE and spatial correlations of extreme event frequency and dry days simulated by all members of the

NARCCAP ensemble are higher than the corresponding values of CCSM3-RegCM3 ensemble members. Several NARCCAP ensemble members have lower spatial variability of total precipitation and mean, extreme, and non-extreme precipitation intensities, although the RMSE and spatial correlations are comparable to the CCSM3-RegCM3 ensemble. However, both ensembles are unable to simulate the spatial characteristics of extreme precipitation fraction with

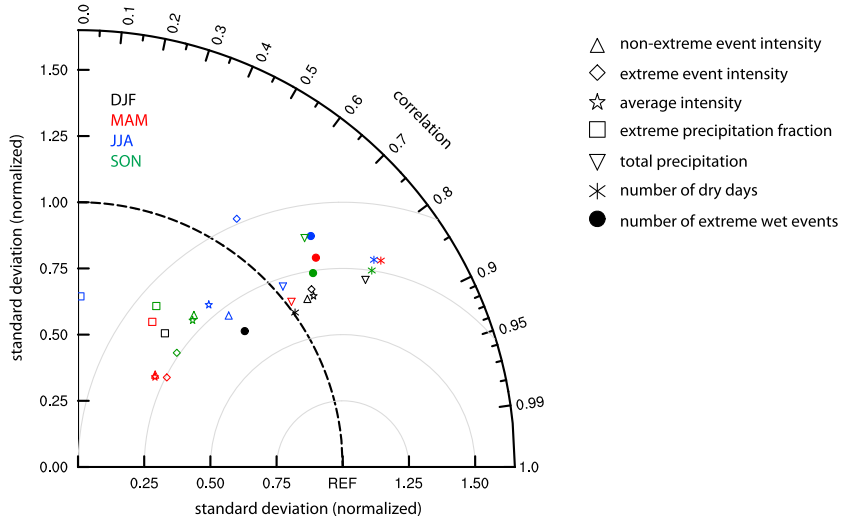


Figure 3. Taylor diagram for seasonal extreme precipitation metrics over the continental U.S. in the present simulations (CCSM3-RegCM3) using CPC precipitation observations as reference. Evaluation is performed for the baseline period (1970–1999). Symbols represent the metrics, and colors represent the season.

accuracy. *Wehner* [2013] also shows that both NCEP- and GCM-driven regional models in the NARCCAP ensemble have substantial variation in their skill to represent precipitation. Specifically, most of these models demonstrate a wet bias in simulating extreme precipitation characteristics. These ensembles are used to further to assess two different sources of uncertainty in projections, namely, internal variability and model uncertainty [*Hawkins and Sutton*, 2009, 2011]. Therefore, this comparison does not quantify the relative skill of the two ensembles.

[22] Next, we analyze biases in seasonal precipitation metrics simulated by the CCSM3-RegCM3 ensemble (Figure 3). The most prominent seasonal precipitation biases (Figure S4) include excessive winter, spring, and autumn precipitation over the mountainous regions in the Northwest and low-elevation regions in California. Additionally, strong dry biases exist in summer and autumn precipitation over the Southeast and southern Great Plains. The ensemble simulates excessive number of rain days in winter and spring across the U.S. and underestimates rain days in most of southern and central U.S. in summer. Biases in the frequency of seasonal wet extremes are small in most regions except the Northwest in winter, spring, and autumn and the southwest and southeast in summer. However, their intensity shows a wet bias in the mountainous and low-elevation regions in the western U.S. in winter, spring, and autumn. It also shows a dry bias in the eastern U.S. in spring and autumn and in the southern Great Plains in summer. The seasonal extreme precipitation fractions are underestimated in most regions. Figure 3 summarizes the performance of average seasonal biases for all the metrics in each season. The RMSE for all metrics are comparable. The simulations have a high spatial correlation (exceeding 0.6) with the observed seasonal precipitation metrics (except extreme precipitation fraction) over the continental U.S. Additionally, the observed spatial variability of the metrics in all seasons is accurately captured. Significant exceptions to this include the variability of extreme precipitation fraction in all seasons; the number of dry days in spring, summer, and autumn; and precipitation intensities in spring and autumn.

3. Results

3.1. Annual Extremes

[23] Figure 4 shows the 21st century evolution of changes in total annual precipitation, number of extreme wet events, and dry-day occurrence. Total annual precipitation shows a general pattern of negative anomalies in the lower latitudes and positive anomalies in the higher latitudes. In the near term, parts of the Southwest exhibit significant decreases in precipitation of up to 15%. This drying intensifies through the 21st century over most of the Southwest, southern Great Plains, and northern Mexico, exceeding 35% in parts of the Southwest by the late 21st century. Moderate increases in total precipitation (~15 to 20% by 2070–2099) are confined to coastal areas of the Northeast and mountainous areas of the Northwest. These positive precipitation changes become statistically significant in the mid- to late 21st century.

[24] Increases in both wet and dry extremes become significant over many parts of the U.S. as early as 2040–2069 (Figure 4). Wet extremes increase in the northern regions, in particular over the northern Rockies and Cascades in the western U.S., and along the Atlantic coast. In the Northeast, anomalies in the frequency of wet events reach 15–20% as early as 2010–2039, exceed 25% in 2040–2069, and expand over a much larger region in 2070–2099. Likewise, by the late 21st century, the occurrence of wet extremes exceeds 50% over parts of the Northwest. These anomalies correspond to approximately six more extreme wet events per year in 2070–2099 than in 1970–2099 in the mountainous areas of the Northwest and coastal areas of the Northeast.

[25] Positive anomalies in dry days occur over most regions of the continental U.S. by the late 21st century, with the greatest increases (up to 14%) occurring over high-elevation areas of the western U.S., along the Gulf of Mexico, and over parts of the Midwest. These anomalies correspond to approximately 32 more dry days annually in 2070–2099 than in 1970–2099. Significant changes of 6–8% occur over parts of the Northwest and the Appalachians in 2010–2039 and over most areas of the eastern U.S. by 2040–2069. These results

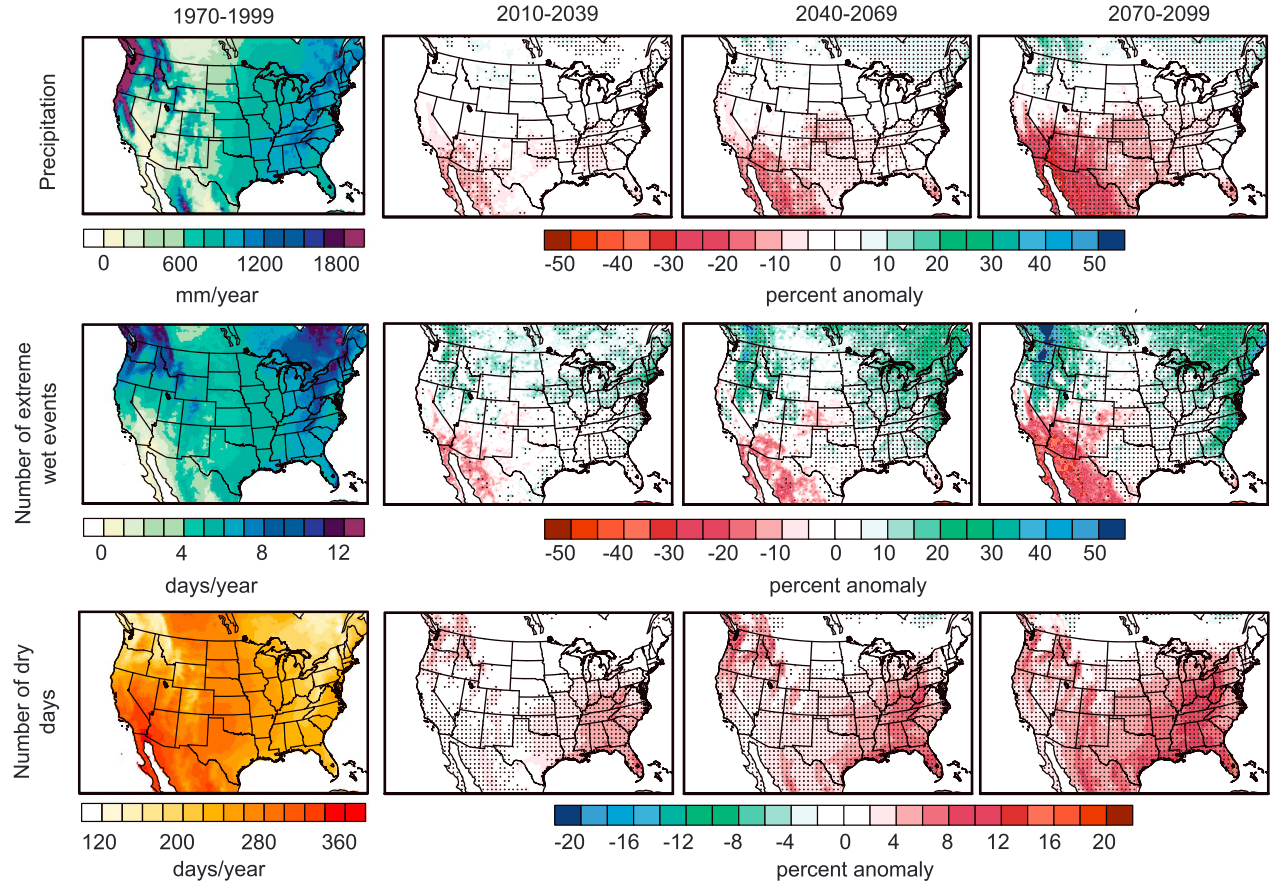


Figure 4. Anomalies (expressed as a percent) in (top) total annual precipitation, (middle) extreme wet events, and (bottom) dry days in 2010–2039, 2040–2069, and 2070–2099 (second through fourth columns) relative to the baseline (1970–1999) values (shown in the first column). Stippling indicates areas that experience a change that is significant at the 5% level.

suggest that the increases in wet extremes seen over much of the Northeast and Northwest occur in conjunction with decreases in total rain days. It can therefore be inferred that the ratio of the occurrence of extreme events to total rain days increases over most regions by the end of the 21st century.

[26] Figure 5 presents the changes in extreme precipitation fraction in 2070–2099 relative to 1970–1999. The extreme precipitation fraction is a function of the ratio of wet extremes to total rain days and extreme to average precipitation intensity. Anomalies in extreme precipitation fraction are positive over most areas of the Northwest and most regions of the Atlantic coast, including positive anomalies exceeding 30% over areas that experience decreases in total precipitation (such as the south-central states and parts of the Midwest; Figure 4). Significant increases in extreme precipitation intensities of 8–10% are confined primarily to areas of the eastern U.S., with a maximum increase of 16–20% over the Southeast (where the intensity is >36 mm/day in the baseline) (Figure 5). Anomalies in the average precipitation intensity exceed 10% in most regions of the U.S., excepting the Southwest and Great Plains. The intensity of non-extreme events also increases by 6–8% over some areas where the overall precipitation change is also positive (primarily in the Northwest). Consequently, the ratio of extreme precipitation intensity to average precipitation intensity decreases over most regions in the future relative to the baseline

(with the exception of Florida and the high-elevation regions in northern Mexico). Thus, the extreme precipitation fraction increases primarily due to a greater fraction of extreme wet events relative to the total number of rain days and not due to an increase in the intensity of extreme events. (This interpretation is not affected by the significance screening applied in the above results.) Indeed, Florida is the only area where positive anomalies in extreme precipitation fraction result from increases in both the fraction of wet extremes in total rain days and their intensity.

[27] Next, we examine the simulated changes in the daily precipitation distribution (Figure 6) over the six regions (refer to Figure 1). It is evident that the frequency of dry days increases, the frequency of low-precipitation events (<16 mm/day) decreases, and the frequency of heavy precipitation events (>16 mm/day) increases in all regions in the late 21st century, with the exception of the Southwest. In the Southwest, the drying pattern (Figure 4) is reflected in lower frequencies across almost all bins, although occurrence does increase moderately in the wettest bins (>48 mm/day). The Northeast experiences the greatest positive anomalies in the frequency of precipitation events, with increases in the heaviest precipitation bins exceeding 50% within the near-term period. Strong positive anomalies in the frequency of moderate to heavy precipitation events also occur in the Southeast, Northwest, Midwest, and Great Plains, with

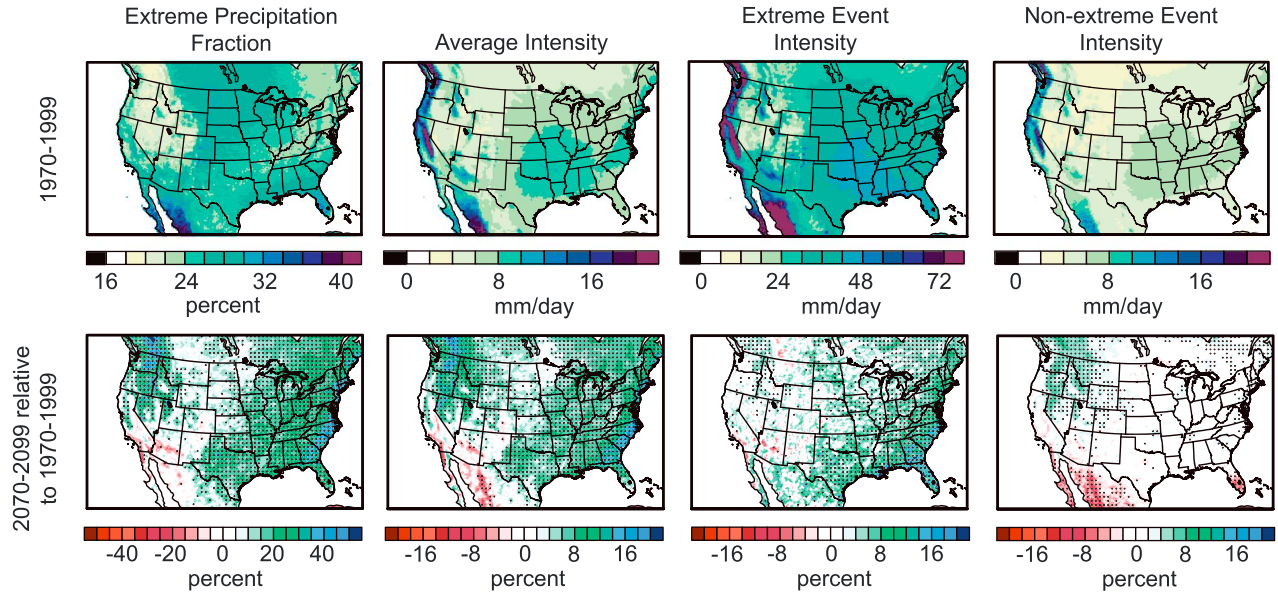


Figure 5. Anomalies in extreme precipitation fraction of total annual precipitation (first column), average precipitation intensity (second column), intensity of extreme events (third column), and intensity of non-extreme events (fourth column) in 2070–2099 relative to the baseline period (1970–1999) values (top). All events with precipitation greater than 1 mm and lesser than the 95th percentile value are referred to as non-extreme events. Stippling indicates areas that experience a change significant at the 5% level.

changes in the heavier precipitation bins exceeding 25% by the mid-21st century.

[28] Further, we find changes in the occurrences of consecutive wet and dry extreme events (Figures 7 and 8). There are few changes in the frequency of consecutive wet events that exceed one standard deviation of intra-ensemble spread, implying low signal-to-noise ratio (Figure 7). However, the frequency of long dry spells increases consistently in all regions over the course of the 21st century, with the exception of the Northeast (Figure 8). Substantial increases in the frequency of dry spells of duration greater than 200 days occur over the Southwest by the end of the 21st century. In wetter regions like the Southeast and the Northwest, shorter duration dry spells (over 60 days) exhibit increases in occurrence that exceed one standard deviation of the intra-ensemble spread in the late 21st century.

3.2. Total Seasonal Precipitation

[29] The pattern and magnitude of seasonal precipitation changes generally emerge early in the 21st century simulations and intensify as radiative forcing increases through the century (Figure 9). The most robust seasonal-scale anomalies in the near-term (2010–2039) period include a significant reduction of approximately 25–30% in summer precipitation in the southern Great Plains; 20–25% increases in summer precipitation in the Northeast; 25–30% increases in spring precipitation in the northern Great Plains, and 10–20% drying in the Southeast in winter and spring.

[30] The pattern of precipitation change varies between the seasons (Figure 9). Winter (December–January–February) precipitation increases in the northern Great Plains, Canada, and parts of the Northwest, with many areas in the southern U.S. experiencing a progressive drying trend through the 21st century. In the winter, negative anomalies of up to

20% occur in the southwestern and southeastern U.S. in the mid-century and intensify to at least 30% over a larger area by 2070–2099. In spring (March–April–May), areas of the southwestern and southeastern U.S. experience significant negative anomalies, while much of the northern parts of the domain experience consistent positive anomalies. These positive anomalies are of the order of 20% in the northern Great Plains in the early part of the 21st century and exceed 30% over most parts of the northern Rockies, northern Great Plains, and Canada by the end of the century. Substantial decreases in summer (June–July–August) precipitation (>30%) are found over the Great Plains, Midwest and Southwest by the mid-21st century and over most of the central and western U.S. by the late 21st century. Additionally, positive anomalies (~25%) in summer precipitation emerge in the Northeast during the mid-to-late century. In autumn (September–October–November), the Southwest and northern Mexico experience significant drying, including negative precipitation anomalies that exceed 35% by 2070–2099. Further, moderate increases (>20%) in precipitation occur over the Northwest and western parts of Canada in autumn by the mid-21st century.

3.3. Regional Precipitation Distributions

[31] As with the annual precipitation distribution, we examine the seasonal precipitation distributions within the six regions. Five of the six regions show qualitatively similar changes in seasonal precipitation distribution, with the Southwest region being an outlier. For illustrative purposes, we focus here on results from the Southeast and Southwest regions (Figures 10 and 11). The pattern of increases in the frequency of moderate to heavy events (precipitation >16 mm/day) and decreases in the frequency of lower-intensity events (precipitation <16 mm/day) is consistent in all the regions except the Southwest, with the magnitude

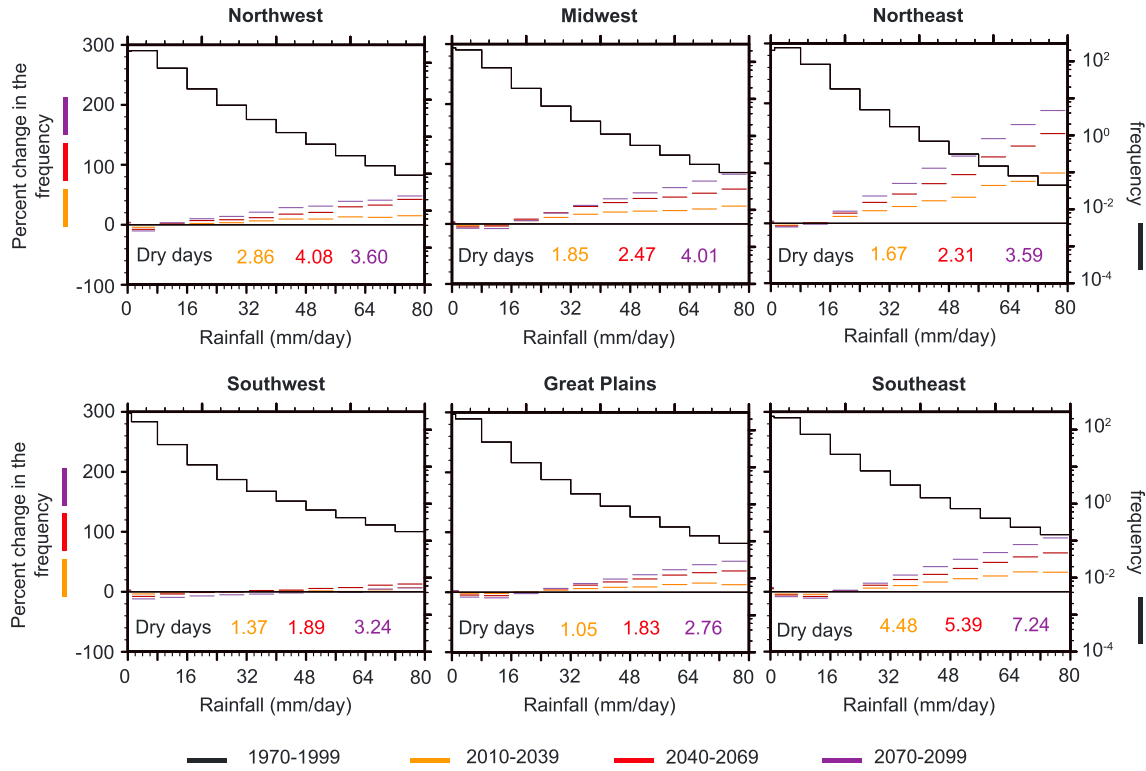


Figure 6. Percent changes in the regional annual precipitation distributions in 2010–2039 (yellow), 2040–2069 (red), and 2070–2099 (purple), relative to the baseline(1970–1999) precipitation (black lines). The frequency of precipitation events (per year) in the baseline is presented on a log scale shown on the right in each figure. The colored numbers on the precipitation distribution figures represent the percentage change in the number of dry days (precipitation between 0 and 1 mm) in each future time period.

of the change in distribution intensifying consistently throughout the 21st century (Figure 10). The largest relative changes in the frequency of the heavy rainfall events are observed in the autumn season, when the Southeast experiences substantial increases in the frequency of events exceeding 40 mm/day, including increases of approximately 50% in 2010–2039 and 200% in 2070–2099. Relative anomalies in summer precipitation distribution are also substantial in the Southeast, Northeast, Midwest, Great Plains, and Northwest regions, with positive anomalies exceeding 100% in the very heavy events by the late 21st century. In contrast, the winter and spring seasons experience increases of up to 25–50% in the frequency of heavy events by the end of the 21st century.

[32] The Southwest region shows a contrasting pattern of change in the seasonal precipitation distribution (Figure 11). The robust and significant decreases in seasonal precipitation in the Southwest (Figure 9) are reflected in a consistent decrease in the frequency of almost all precipitation bins throughout the year in the late 21st century. However, the winter and spring season distributions show some nonmonotonic changes with time, with increases (<10%) in moderate to heavy events in the early 21st century period and decreases (<10%) of moderate to heavy events in the late 21st century period. Consistent with the intense drying in the region, occurrences of summer and autumn precipitation events decrease progressively in the 21st century, with the exception of the very heavy events (>56 mm/day) in autumn.

3.4. Precipitation Extremes

[33] The changes in the distribution of precipitation during the four seasons (Figures 10 and 11) indicate an increase in the frequency of dry days, a decrease in the frequency of low-precipitation events (<16 mm/day), and an increase in the frequency of moderate to heavy events (>16 mm/day) in most regions except the Southwest. These changes are consistent with what is expected theoretically in a warmer atmosphere [O'Gorman and Schneider, 2009; Held and Soden, 2006; Allan and Soden, 2008; Giorgi *et al.*, 2011; Trenberth, 1999; Lintner *et al.*, 2012] and are likely to influence the frequency of both wet and dry extreme precipitation events.

3.4.1. Wet Extreme Events

[34] Figure 12 shows future anomalies in the number of days with precipitation exceeding the seasonal baseline 95th percentile value. In many regions, the relative changes in seasonal extremes are greater in magnitude and spatial extent (Figure 12) than the relative changes in annual extremes (Figure 4). The general spatial pattern of change in extreme precipitation occurrence tends to be consistent through the 21st century, with increasing magnitude and extent of change in response to increasing radiative forcing.

[35] The mountainous Northwest exhibits increases in the occurrence of wet extremes exceeding 35% by the mid-21st century in spring, winter, and autumn (Figure 12). Anomalies over these areas intensify further, exceeding 50% by the end of the 21st century. Increases in autumn extreme events are projected to occur primarily in the rain-shadow region between the Cascades and the

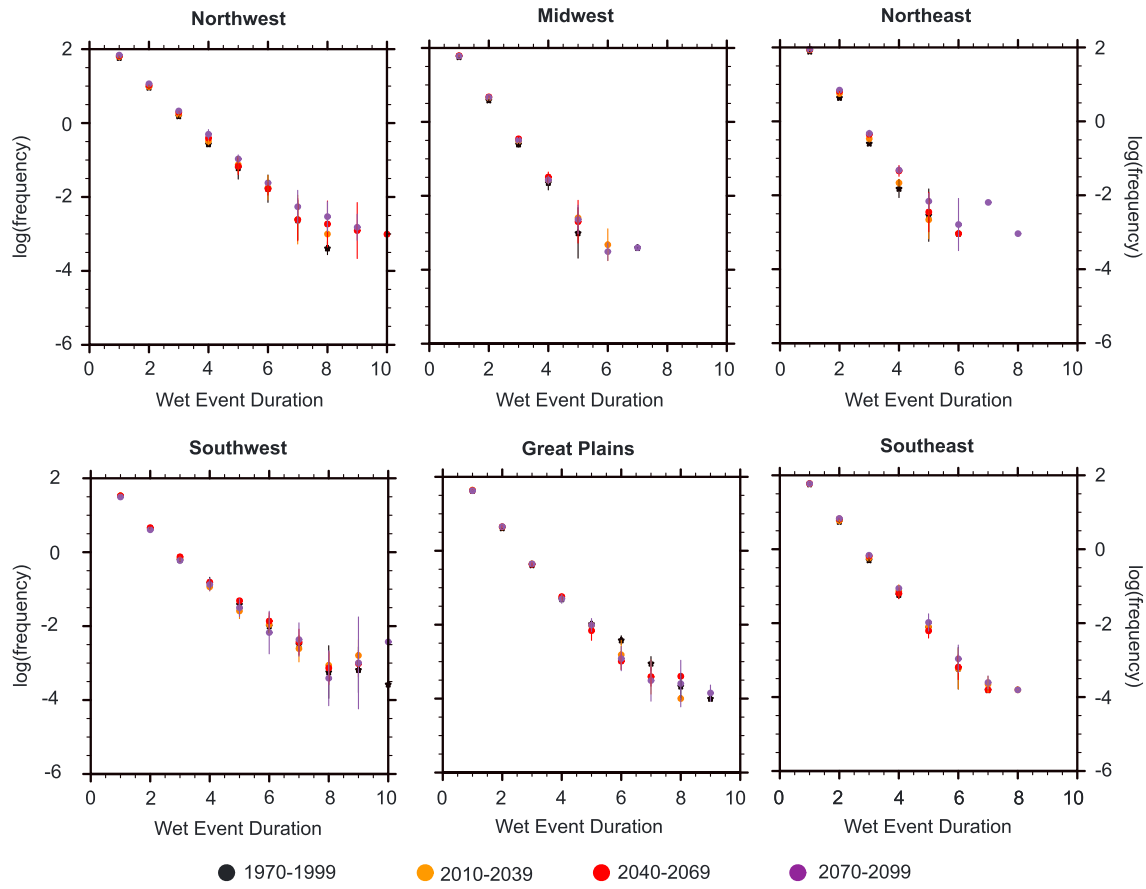


Figure 7. Average frequency (events per year expressed on a log scale) of occurrence of consecutive wet extremes in 2010–2039 (yellow), 2040–2069 (red), 2070–2099 (purple), and in the baseline (1970–1999) values (black). The lines indicate ± 1 standard deviation calculated from the ensemble.

Rockies, including anomalies exceeding 50% during the 2070–2099 period. Positive anomalies of over 40% occur on the leeward side of both ranges in winter—and additionally over the high-elevation areas in spring—by the end of the century. Summer extremes become more frequent over most areas along the Atlantic coast in response to warming. Large positive anomalies exceeding 50% occur in the coastal Northeast by the mid-21st century, and amplify in the late 21st century. Most areas that exhibit increases in the occurrence of wet precipitation extremes also exhibit increases in total precipitation (Figures 9 and 12). However, there are some regions that experience increases in wet extremes without any significant changes in the total precipitation, such as the coastal Southeast in summer, and parts of the Midwest and eastern U.S. in spring.

[36] Negative anomalies in the occurrence of wet extremes occur in some areas of the U.S. that experience significant overall drying and a reduction in the frequency of low and heavy precipitation events (Figure 12). For example, the frequency of wet extremes reduces by up to 40% in the Southwest and northern Mexico in autumn and winter in the late 21st century period. Some of these autumn season changes emerge as early as the mid-21st century period. Also, the southern Great Plains and parts of northern Mexico exhibit 35–40% fewer wet extremes in summer by mid-century, with negative anomalies expanding over the western U.S. in the late 21st century.

3.4.2. Dry Days

[37] Figure 13 shows changes in the occurrence of dry days in each season in the 21st century. We find significant positive anomalies in dry-day occurrence in all seasons in all three 21st century periods, with the largest and most widespread changes occurring in winter and summer. Robust near-term changes (>8%) are seen in many parts of the U.S. in winter, spring, and summer, with the greatest spatial extent occurring in summer. The pattern of change that emerges in the near-term period intensifies and expands through the 21st century.

[38] In the winter season, dry-day anomalies mostly occur in the western U.S., northern Mexico, and the Southeast, including changes greater than 12% over the mountainous areas of the western U.S. by 2070–2099 (Figure 13). In summer, all regions of the U.S. exhibit increases in the frequency of dry days during the mid-21st and late 21st century, with the exception of the Southwest. Increases of over 12% in the summer dry-day frequency occur over most areas of central and eastern U.S. by the mid-century, with changes exceeding 20% over some parts of the Gulf of Mexico, Appalachians, and Great Plains by 2070–2099. Spring and autumn dry days also exhibit moderate changes by the late 21st century, including increases of approximately 10% over parts of the eastern U.S., Midwest, and southwestern U.S. in spring and the Rockies, the Northeast, and northern Mexico in autumn.

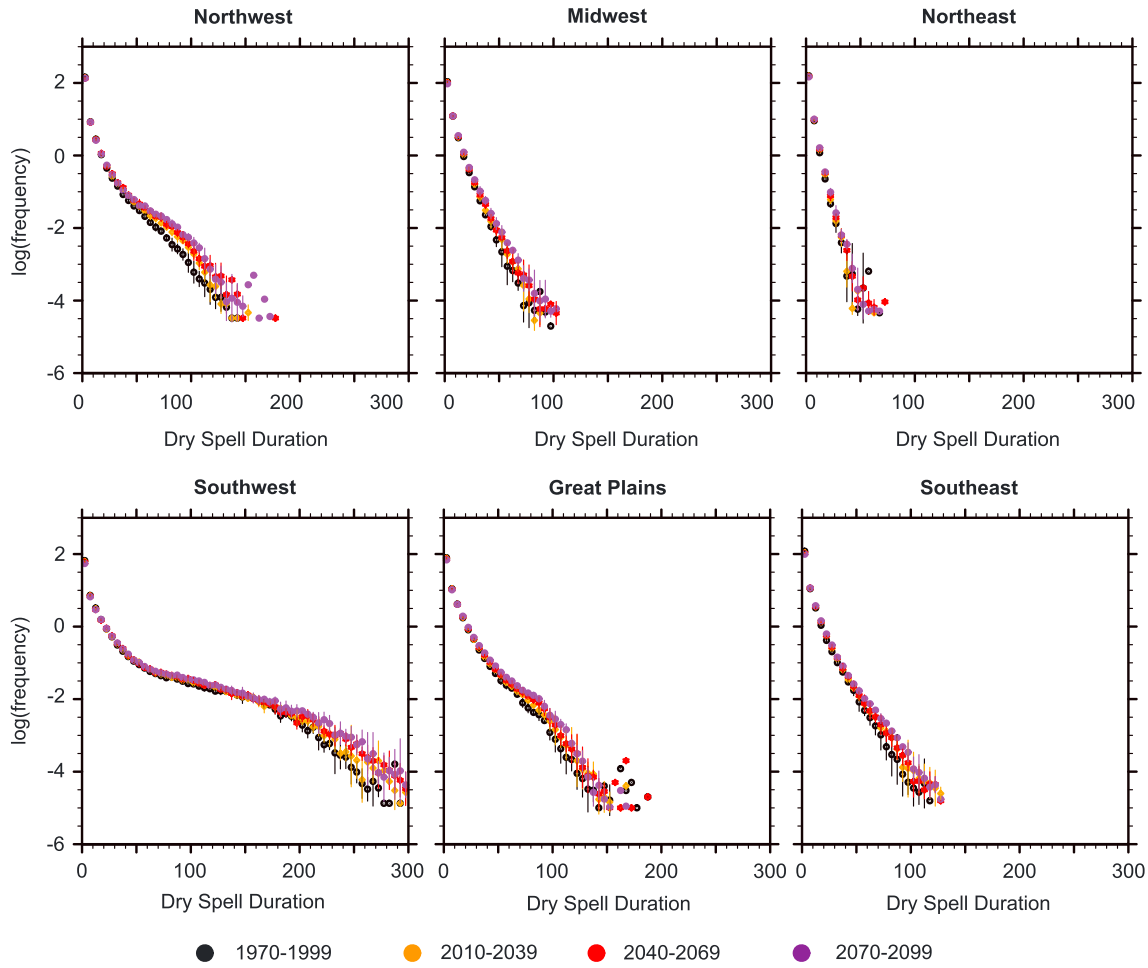


Figure 8. Same as in Figure 7 but for consecutive dry days.

[39] Negative anomalies in dry-day frequency are confined primarily to the winter and spring seasons (Figure 13). Significant decreases of 10–14% are found mostly in Canada and parts of the Northeast in winter and over the northern Rockies in spring during 2070–2099.

3.5. Analysis of Extreme Precipitation Contribution and Precipitation Intensity

[40] Co-occurrence of increases in both wet extremes and dry-day frequency occur over many areas of the continental U.S., including the Atlantic coast in summer, the Midwest in spring, and the western U.S. in winter, suggesting an intensification of both wet and dry conditions. Given the projected changes in both wet and dry extremes, we quantify the influence of global warming on the intensity precipitation events and the contribution of precipitation extremes in total seasonal precipitation.

[41] Figure 14 shows the extreme, non-extreme, and average precipitation intensities and extreme precipitation fractions in the baseline period. Average baseline extreme precipitation fractions exceed 26% over the Great Plains and southern U.S. in spring; central, eastern, and southwestern U.S. in winter and autumn; and over most of the continental U.S. in summer.

[42] Significant increases in extreme precipitation fraction predominantly occur over the Atlantic coast and the

Northwest by the end of the 21st century, including changes that exceed 50% in the summer and 25% in the spring along the Atlantic coast (Figure 15). The extreme event intensity increases by 16–20% over a few scattered areas of the eastern U.S. during these seasons. The intensity of non-extreme events also increases (>8%) in parts of the Northeast in summer, leading to a comparable or greater increase in the average precipitation intensity. As a consequence, the ratio of extreme to average precipitation intensity decreases in these regions, with the exception of a few locations in the Southeast. However, the increasing frequency of wet extremes (40–50%) relative to the total rain days in these regions results in higher extreme precipitation fraction in most parts of the eastern U.S. in spring and summer. In the Southeast, the extreme precipitation fraction increases due to an increase in both the fraction of wet extremes and the extreme precipitation intensity in summer.

[43] In parts of the Northwest, extreme precipitation fraction increases by over 40% in autumn, winter, and spring in 2070–2099 relative to the baseline. The ratio of extreme to average precipitation intensity decreases in the late 21st century as a result of increases (12–20%) in average precipitation intensities over the mountainous Northwest, with relatively few changes in extreme precipitation intensity. The intensity of non-extreme events also

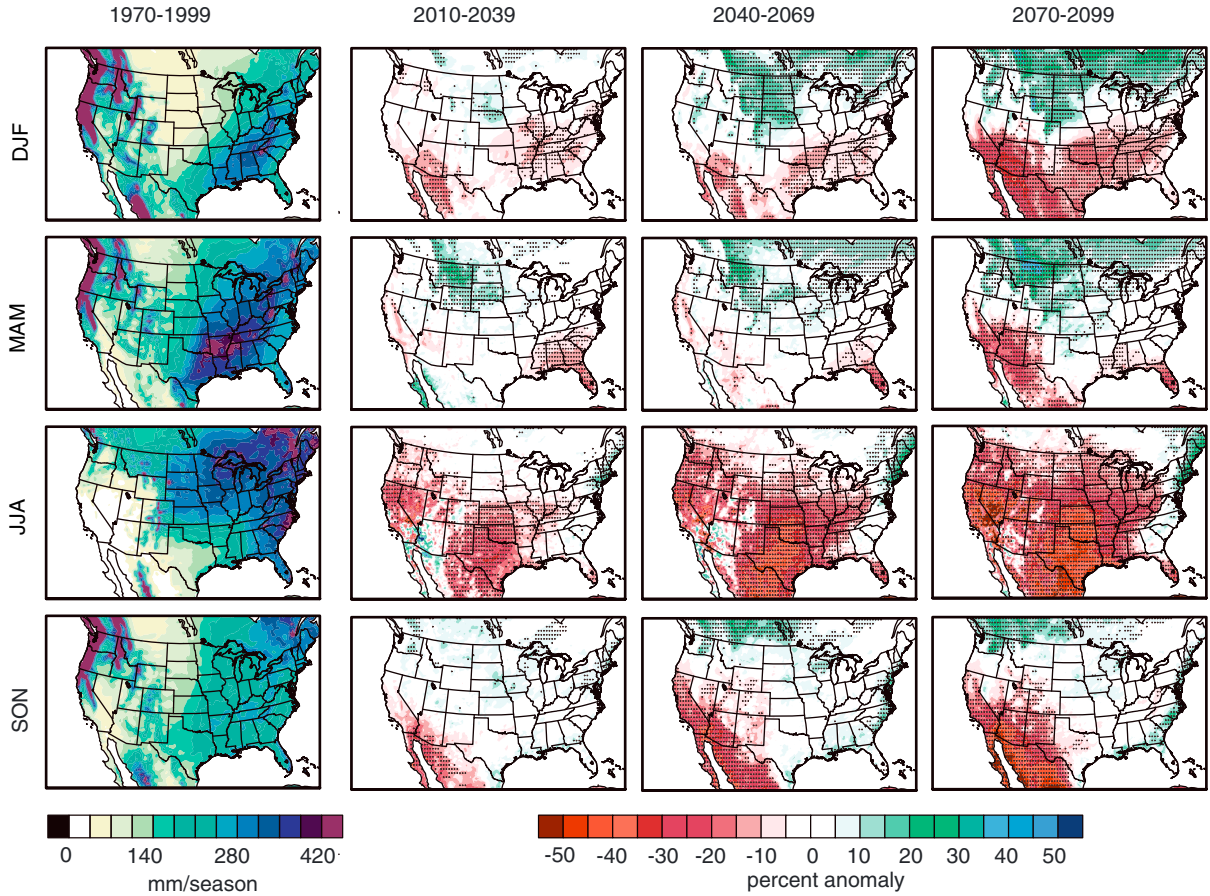


Figure 9. Seasonal precipitation anomalies in 2010–2039, 2040–2069, and 2070–2099 (second through fourth columns) relative to the baseline (1970–1999) precipitation (shown in the first column). Stippling indicates regions where the change is significant at the 5% level.

increases by 10–12% in the Intermountain Regions, where there is an increase in autumn precipitation. However, positive anomalies in the occurrence of wet extremes exceeding 30% and fewer rain days in most seasons (dry extremes increase by >12% in winter) result in increases in the fraction of extreme wet event occurrence in the Northwest. This increasing fraction of extreme wet events leads to the increase in extreme precipitation fraction in the region.

[44] Similarly, moderate increases of approximately 20–30% in the extreme precipitation fraction in spring, summer, and autumn occur over the Midwest. Likewise, the average precipitation intensities over the region increase by a magnitude greater than the extreme precipitation intensities. Dry days increase by over 12% in spring, 16% in summer, and 4% in autumn; and wet extremes increase by 20% in spring. Consequently, the fraction of wet extremes increases, whereas the ratio of intensities decreases in the long-term in all seasons.

[45] Overall, this analysis indicates that the increases in extreme precipitation fraction over most parts of the U.S. are primarily a consequence of the increasing ratio of extreme event days to total rain days. Anomalies in average precipitation intensity exceed changes in extreme precipitation intensity over most regions.

4. Discussion

4.1. Processes Shaping Changes in Extremes

[46] Our results show annual- and seasonal-scale changes in the daily precipitation distributions across all regions of the contiguous U.S. in response to transient increases in greenhouse gas concentrations. Overall, the pattern reflects a consistent shift toward increases in moderate to heavy precipitation events, decreases in low-precipitation events, increases in dry days, and lengthening of dry spells. These results are consistent with the expected response to increases in atmospheric moisture content and its saturation vapor pressure with rising atmospheric temperatures [Trenberth, 1999; Trenberth *et al.*, 2003; Giorgi *et al.*, 2011]. Further, we find substantial seasonal and spatial heterogeneity in the pattern and magnitude of extreme precipitation response to warming. This heterogeneity in the response results from the complex interaction of governing large-scale atmospheric processes and local-scale factors that influence precipitation intensity and variability.

[47] Several regions exhibit an enhancement of both wet and dry extremes (Figures 12 and 13), similar to that reported by Lintner *et al.* [2012] for monthly precipitation extremes over the tropics and Lau *et al.* [2013] for daily extremes across the globe. Increases in daily precipitation variability

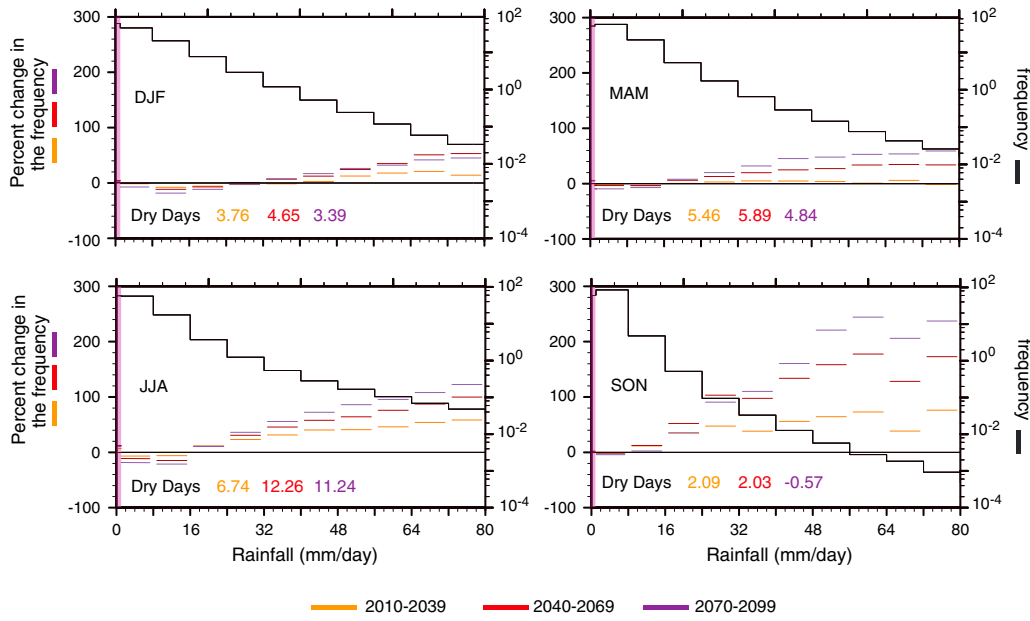


Figure 10. Relative changes in the precipitation distributions in 2010–2039 (yellow lines), 2040–2069 (red lines), and 2070–2099 (purple lines) compared to the baseline (1970–1999) precipitation (black lines) distribution in each of the four seasons in the Southeast. The numbers on each figure represent the percentage change in the number of dry days (precipitation between 0 and 1 mm) in each future time period. The shaded region in each plot also highlights changes in dry days.

(Figure 16) in addition to changes in mean precipitation contribute to the enhancement in these regions. Substantial increases in variability are found over the Southeast and Atlantic coast in summer, the northern Rockies in winter, and most areas of the central and northwestern U.S. in spring. These regions also correspond to

areas of greatest increase in wet extremes and dry days in those respective seasons. In contrast, the Southwest and northern Mexico experience an increase in the occurrence of dry days in autumn, winter, and summer, despite lower precipitation variability, due to decreases in seasonal precipitation.

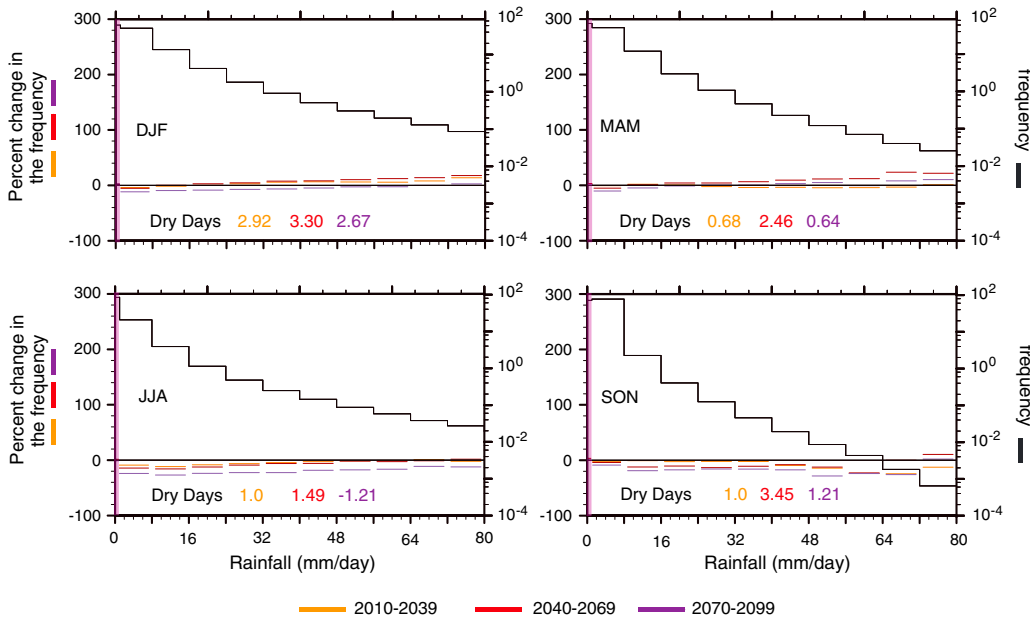


Figure 11. Relative changes in the precipitation distributions in 2010–2039 (yellow lines), 2040–2069 (red lines), and 2070–2099 (purple lines) compared to the baseline (1970–1999) precipitation (black lines) distributions in each of the four seasons for the Southwest. The numbers on each figure represent the percentage change in the number of dry days (precipitation between 0 and 1 mm) in each future time period. The shaded region in each plot also highlights changes in the number of dry days.

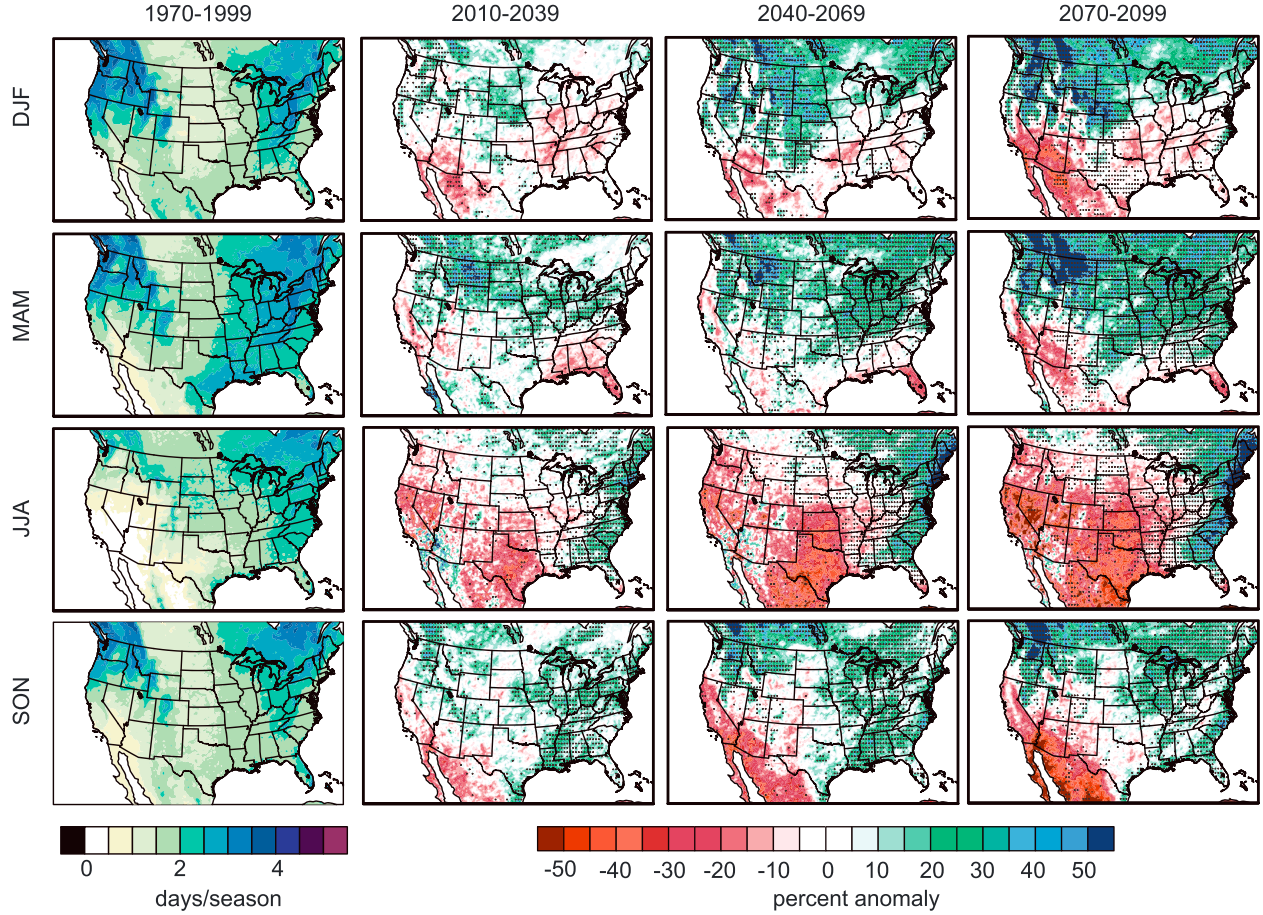


Figure 12. Percent changes in the frequency of seasonal extreme wet events in three future time periods 2010–2039, 2040–2069, and 2070–2099 (second through fourth columns) relative to the baseline (1970–1999) values (first column). Threshold for a seasonal extreme event is defined by the 95th percentile precipitation in each season in the baseline. Stippling indicates regions where the change is significant at the 5% significance level.

[48] The annual and seasonal mean precipitation anomalies (Figures 4 and 9) both show a 21st century pattern of statistically significant increases in precipitation in the high latitudes and statistically significant decreases in the subtropics, similar to previous studies [Meehl *et al.*, 2005; Tebaldi *et al.*, 2006; Wehner, 2013]. The primary exceptions occur during the summer season, which shows widespread drying in most of the U.S. (apart from the Atlantic coast and Southwest). The projected changes in precipitation are a response to enhanced atmospheric moisture content and increased poleward mass transport [Held and Soden, 2006; Emori and Brown, 2005] from the northward shift of the storm tracks [Hall *et al.*, 1994; Yin, 2005; Trapp *et al.*, 2009]. Poleward displacement and intensification of the mid-latitude tropospheric jets is evident across the western, central, and eastern U.S. in most seasons (except winter) at the end of the 21st century (Figure 17). Because precipitation in the western U.S. is dominated by mid-latitude storms associated with the mid-latitude jet, the poleward displacement of the jet results in a pattern of increased precipitation in the Northwest and decreased precipitation in the Southwest. Likewise, poleward displacement of the jet in summer has been associated with decreased baroclinity [Trapp

et al., 2009] and below average precipitation in the central U.S. [Hu and Feng, 2010; Diffenbaugh *et al.*, 2011] (Figure 9).

[49] Next, statistically significant changes in the frequency of both wet and dry extremes occur over some areas of the U.S. in the near-term decades and over most regions by the mid-21st century. These changes in precipitation extremes result from a suite of climate processes. As expected from a warming atmosphere [Trenberth, 1999], the relative increases in the frequency of wet extremes are greater than the increases in mean precipitation, in agreement with previous findings [Giorgi *et al.*, 2011; O'Gorman and Schneider, 2009]. Changes in extremes are proportional to increases in atmospheric moisture content that are affected by atmospheric and sea surface temperatures [Meehl *et al.*, 2005]. Additionally, surface humidity changes (Figure 18) influence precipitation and the occurrence of extremes, particularly in regions where the precipitation is driven by local-scale convective processes. This is evident over the central U.S. where a substantial decrease in specific humidity and relative humidity at the surface (Figures 18a and 18b) in the summer corresponds to the more frequent occurrence of dry days.

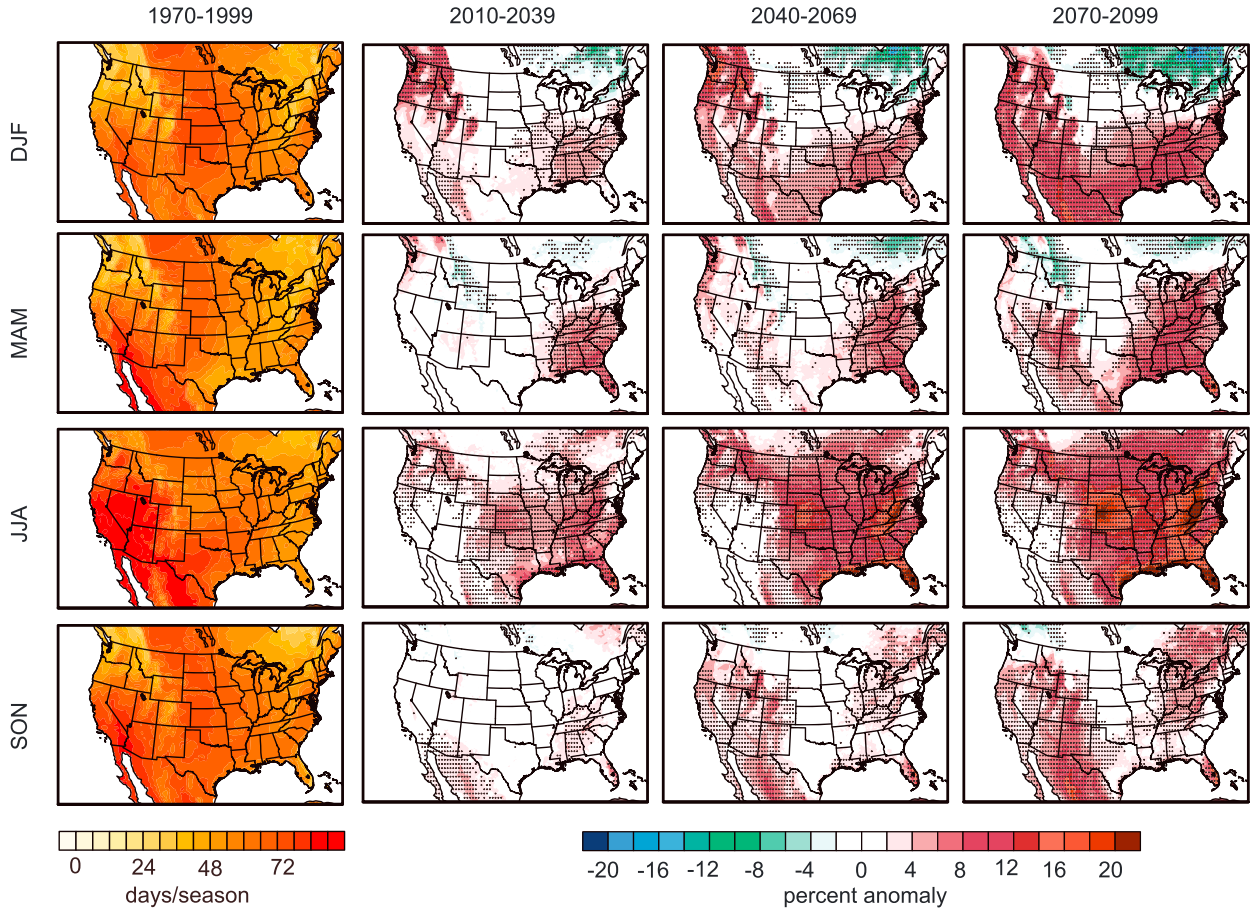


Figure 13. Percent changes in the frequency for seasonal extreme wet events in three future time periods 2010–2039, 2040–2069, and 2070–2099 (second through fourth columns) relative to the baseline (1970–1999) values (first column). Dry days are defined as days with precipitation less than 1 mm.

[50] Further, anomalous circulation patterns can also influence extreme precipitation occurrence by altering storm tracks and atmospheric stability. The most prominent anomalies include intensification of the low-level jet over the Great Plains in spring and summer (Figures 18d and 19). Previous studies have found that the intensification of the low-level jet is associated with the occurrence of wet extreme events over the central U.S. in spring [Trenberth and Guillemot, 1996; Tuttle and Davis, 2006]. However, the existence of the anomalous upper level anticyclonic circulation (Figure 19) in summer increases atmospheric stability and results in reduced convective precipitation over the central U.S. We note that there could be other variables including vertical wind shear [Weisman and Klemp, 1982], pressure gradients [Davies-Jones, 2002], and convective available potential energy [Brooks, 2003] that affect the response of extreme precipitation characteristics to warming.

[51] More frequent heavy precipitation events, along with fewer rain days and fewer low-precipitation events, result in an increase in the extreme precipitation fraction. The average annual and seasonal precipitation intensities show moderate increases over some regions, in accordance with both increases in mean precipitation over the high latitudes and decreases in total rain days in the lower latitudes. Previous studies have also found similar increases in precipitation intensity, extreme precipitation fraction, and dry days in most

midlatitude to high-latitude regions [Tebaldi *et al.*, 2006; Giorgi *et al.*, 2011; Meehl *et al.*, 2005]. Such extreme precipitation fraction changes are associated with increased atmospheric moisture content and changes in atmospheric circulation that increases moisture convergence (Figure 18c) in some regions [Meehl *et al.*, 2005; Diffenbaugh *et al.*, 2005].

4.2. Spatial Patterns of Changes in Extremes

4.2.1. Southwest

[52] The Southwest primarily experiences severe drying in most seasons in response to increased greenhouse forcing (Figure 9). The changes are associated with drier surface conditions (Figure 18) over most of the Southwest in autumn, winter, and spring that result from increased radiative forcing. Consequently, the precipitation distributions in future decades of the 21st century show decreases in the frequency of most precipitation events in all seasons in the Southwest (Figure 11) relative to the baseline. Reduced precipitation and lower daily variability result in consistent increases in the number of dry days (Figure 13) and decreases in the occurrence of wet extremes (Figure 12), respectively. This drying pattern in the Southwest is consistent with previous studies suggesting increasing aridity in the region arising from poleward displacement of the mid-latitude jet (Figure 17) and

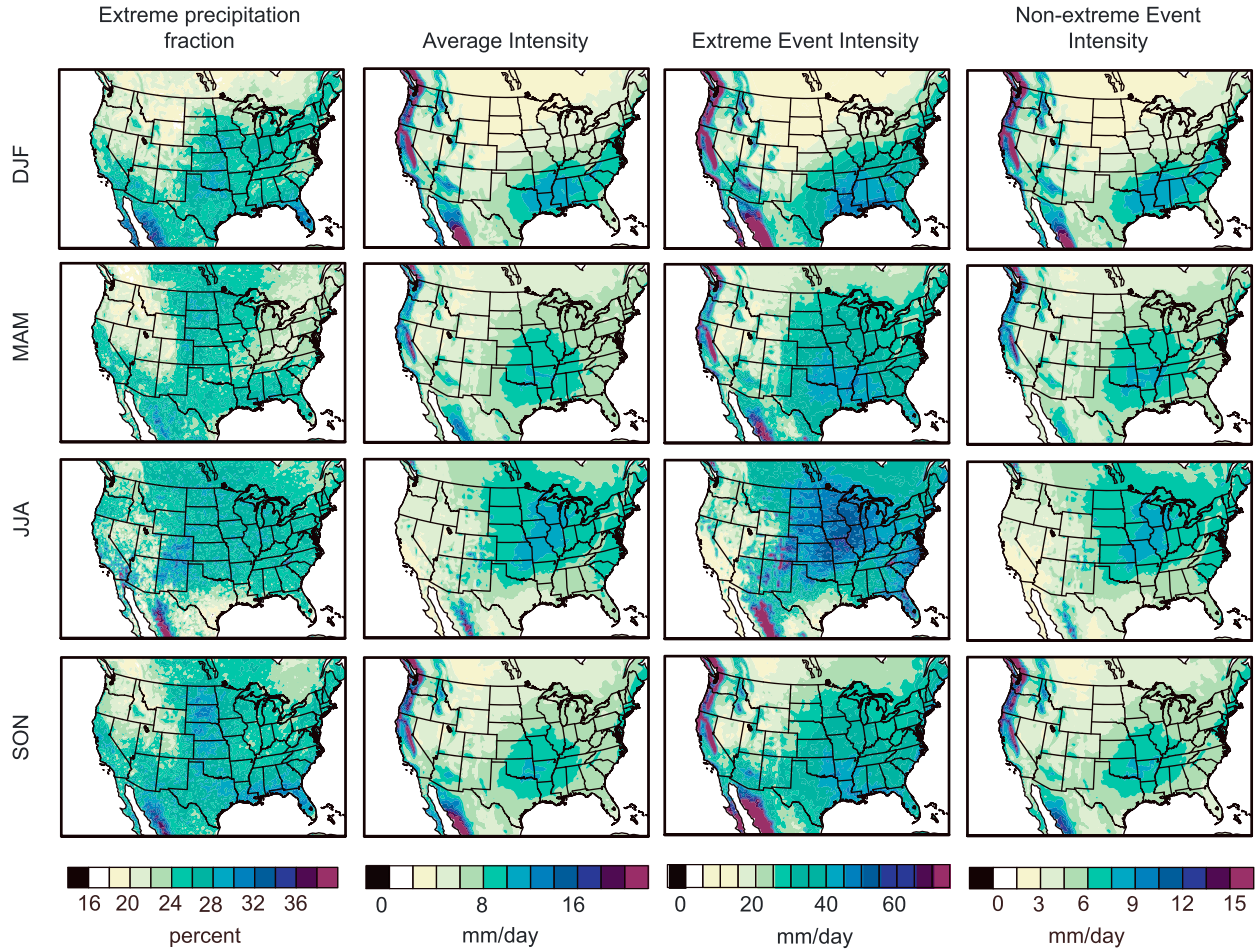


Figure 14. Extreme precipitation fraction of total seasonal precipitation (first column), average seasonal precipitation intensity (second column), extreme events intensity (third column), and intensity of non-extreme events (fourth column) in the four seasons in the baseline (1970–1999).

greater moisture divergence in response to warming [Yin, 2005; Seager et al., 2007; Dominguez et al., 2012].

4.2.2. Northwest

[53] The Northwest experiences substantial increases in autumn, winter, and spring season wet extremes, extreme precipitation fraction, and mean precipitation intensity, predominantly in the Intermountain Regions and leeward side of the Rockies (Figures 12 and 15). This weakening of the rain shadow has also been reported in Difffenbaugh et al. [2005]. These changes are associated with increases in precipitation variability (Figure 16) and northward shift of the midlatitude jet that controls the storm tracks (Figure 17). Further, orographic precipitation and moisture transport across the mountain ranges in the Northwest is enhanced by anomalous upper level cyclonic flow (Figure 19) in winter and spring, in addition to upper tropospheric moisture availability [Difffenbaugh et al., 2005; Meehl et al., 2005]. Consequently, extremes increase in frequency and intensity over the high-elevation and rain-shadow regions of the Cascades and Rocky Mountains in the winter and spring seasons. Our results of increases in extreme precipitation are consistent with previous studies that analyze the high-resolution NARCCAP ensemble over the region [Dominguez et al., 2012; Wehner, 2013].

4.2.3. Northeast

[54] Positive trends in mean precipitation and heavy precipitation events have been noted in the observational record in the Northeast since 1950 [Brown et al., 2010]. We find that this pattern could continue into the 21st century with increased global warming. The poleward shift of the mid-latitude jet over the eastern U.S. (Figure 17) likely contributes to increased precipitation in the region. Positive anomalies in precipitation extremes in the eastern U.S. are largest in the summer, with a moderate increase in extremes along the east coastal U.S. in autumn (Figure 12). Further, increased surface level moisture convergence (Figure 18c) of moist air from over the Atlantic in summer results in an increase in average and extreme precipitation intensity (Figure 15). This is similar to the mechanism suggested by Meehl et al. [2005] for the eastern coastal regions.

4.2.4. Southeast

[55] Increased summer precipitation variability associated with increased moisture availability results in an enhancement of both wet and dry extremes over the Southeast. Also, more frequent occurrence of summer dry days are likely a consequence of the response of convective precipitation to reduced surface relative humidity (Figure 18b) [Manabe and Wetherald, 1987]. Increased moisture

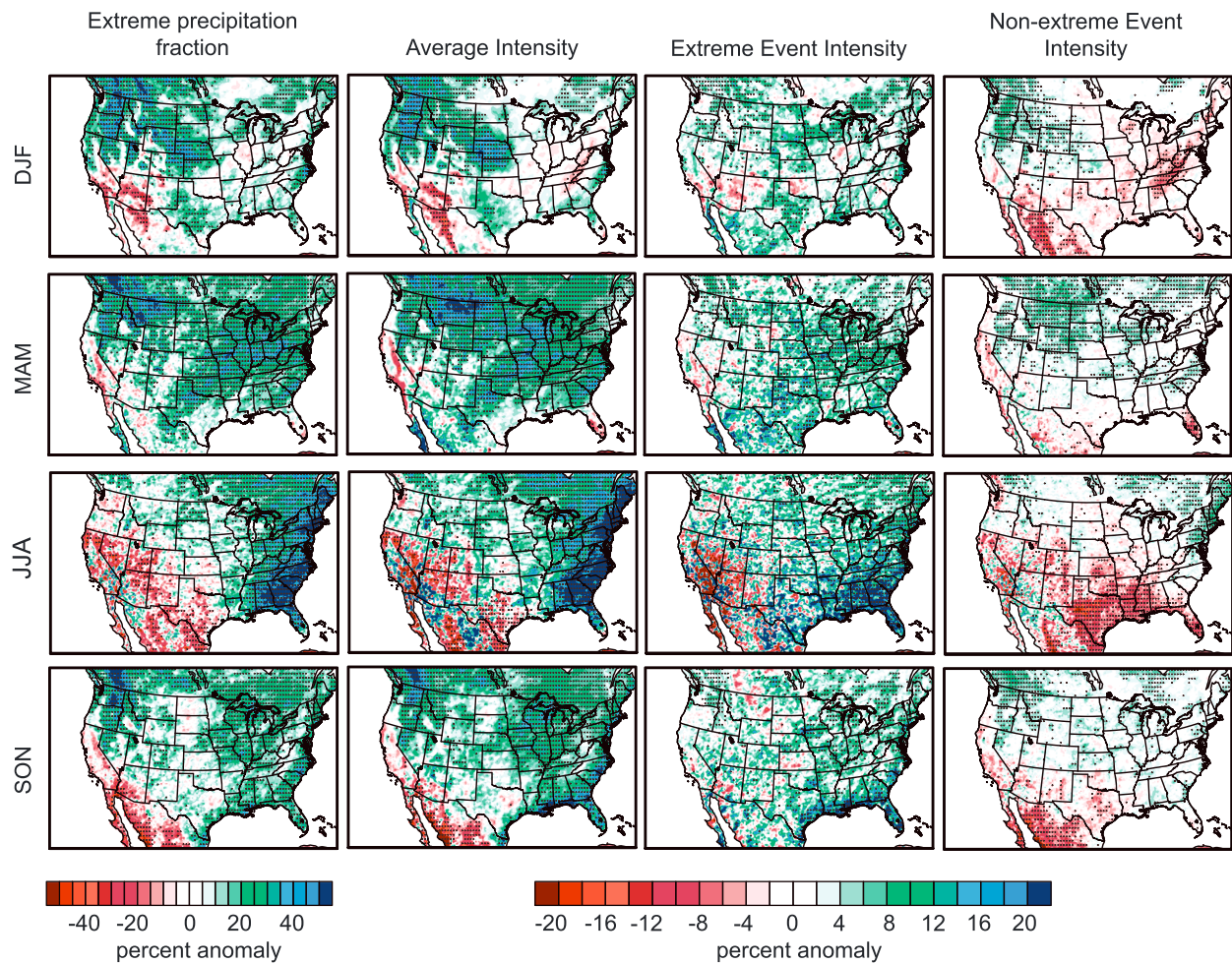


Figure 15. Projected changes in the extreme precipitation fraction of total seasonal precipitation (first column), average precipitation intensity (second column), extreme event intensity (third column), and intensity of non-extreme events (fourth column) in the four seasons in 2070–2099 relative to the baseline (1970–1999) period (shown in Figure 14 for reference). All events in a season with precipitation greater than 1 mm and lesser than the seasonal 95th percentile are referred to as non-extreme events. Stippling indicates regions where changes are significant at the 5% level.

convergence (Figure 18c) in spring and summer and the anomalous cyclonic circulation over the region in summer, results in higher extreme precipitation fraction and increased precipitation intensity [Diffenbaugh *et al.*, 2005].

Further, moderate increases in extreme precipitation fraction and precipitation intensity along the Gulf of Mexico and the Atlantic coast in autumn are associated with the increased low-level moisture convergence (Figure 18c).

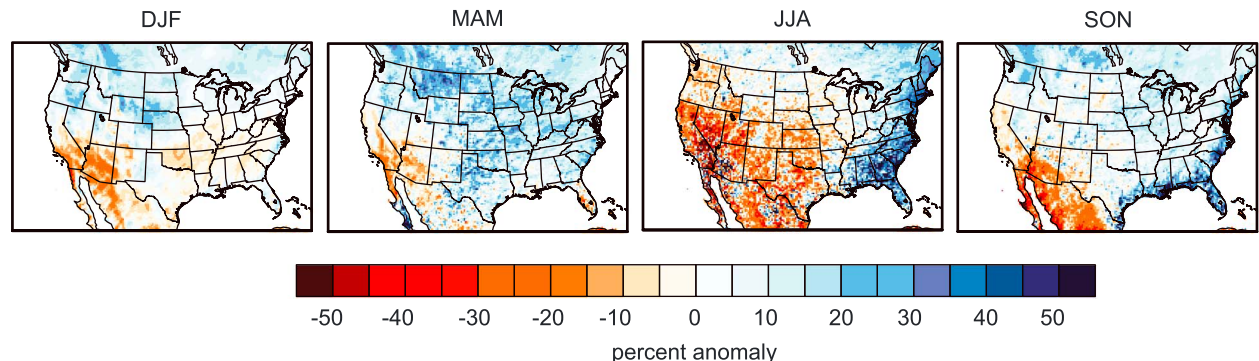


Figure 16. Percent anomalies in the standard deviation (variability) of precipitation in each season in 2070–2099 relative to the standard deviation of daily precipitation in each season in the baseline period (1970–1999).

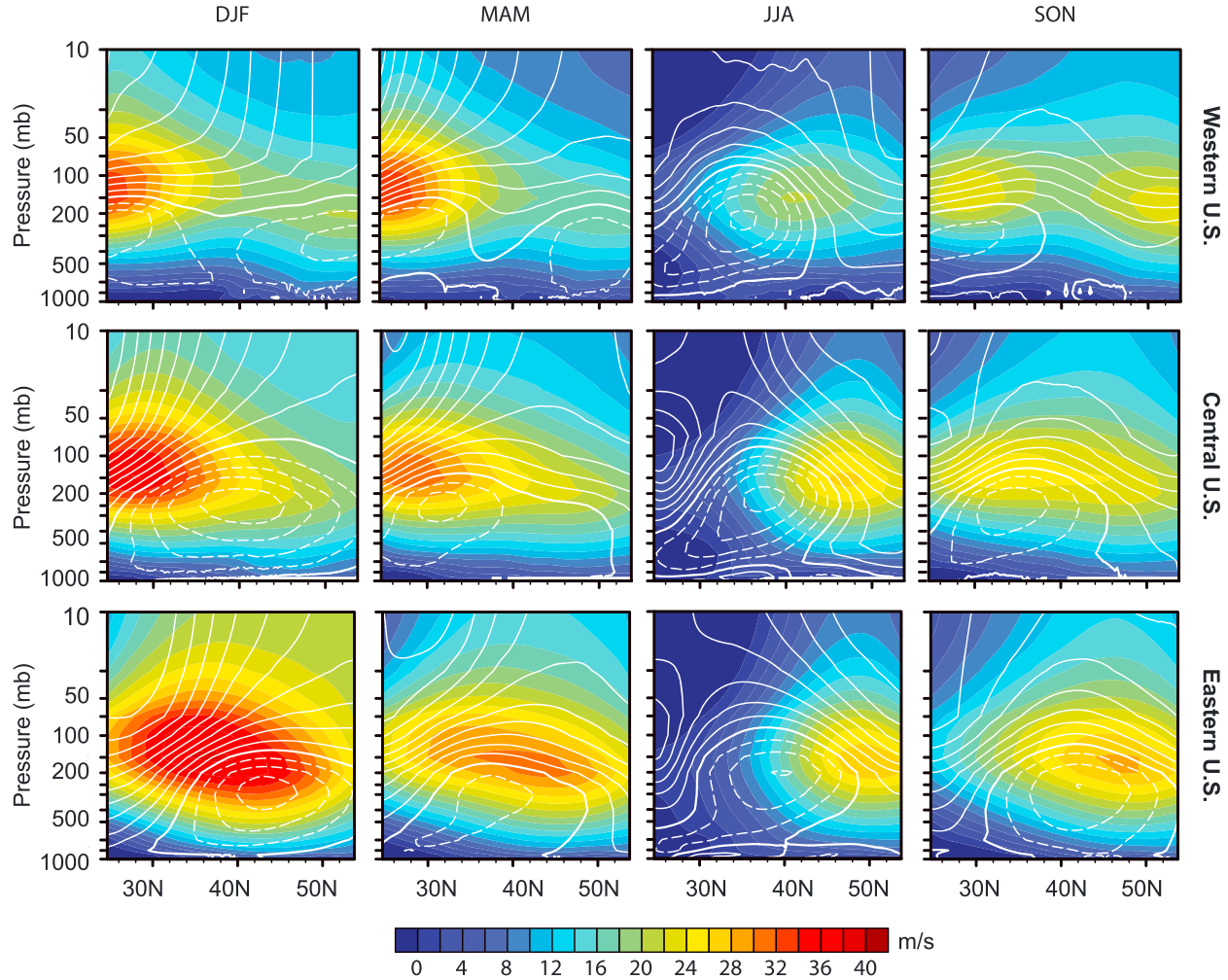


Figure 17. Zonal (U component of the wind) winds (color scale) in the baseline (1970–1999) and anomalies (contour lines, 0.5 m/s intervals; solid lines indicate positive change, thick solid lines indicate no change, dashed lines indicate negative changes) in 2070–2099 relative to the baseline, averaged across the eastern (70°W – 90°W), central (90°W – 110°W), and western U.S. (110°W – 125°W) domains.

4.2.5. Great Plains and Midwest

[56] The most widespread statistically significant changes in extreme precipitation characteristics over the Great Plains and Midwest occur in the winter, spring, and summer (Figure 9, 12, 13, and 15). The low-level jet that carries moisture from the Gulf of Mexico to the Great Plains in spring and summer intensifies in response to warming (Figure 18c) as is also shown by Cook *et al.* [2008]. The low-level jet is a source of moisture for the mesoscale convective systems that initiate over the eastern Rockies. Its strength is correlated with the intensity of rainfall in the region of convergence in the northern Great Plains and the Midwest [Tuttle and Davis, 2006]. Consequently, the increase in extreme precipitation frequency and intensity over these regions in spring results from an increase in moisture convergence over the northern Great Plains (Figure 19) and the suggested increase in severe thunderstorm environments [Trapp *et al.*, 2009] in response to increased radiative forcing. In summer, surface relative humidity decreases substantially over the central U.S. (Figure 18) due to increases in surface sensible heat fluxes

[Diffenbaugh *et al.*, 2011; Manabe and Wetherald, 1987; Wetherald and Manabe, 1995]. In addition, more stable atmospheric conditions associated with existence of the upper level anticyclonic anomaly (Figure 19) leads to widespread drying in the Midwest and Great Plains region in summer. Previous studies have linked the upper level anticyclonic anomaly to drought conditions over the Great Plains [Chen and Newman, 1998; Hong and Kalnay, 2002].

4.3. Caveats

[57] Although our climate model experiment is an unprecedented high-resolution century-scale ensemble in its combination of scope and detail, it does still present a number of limitations. For example, the heavy computational requirement of high-resolution modeling has limited our ensemble to only five ensemble members using a single model. Uncertainty in climate change projections results from both internal climate variability and model-response uncertainty [Hawkins and Sutton, 2009, 2011]. Deser *et al.* [2012] use a 40-member physically uniform ensemble to show the extent of uncertainty in

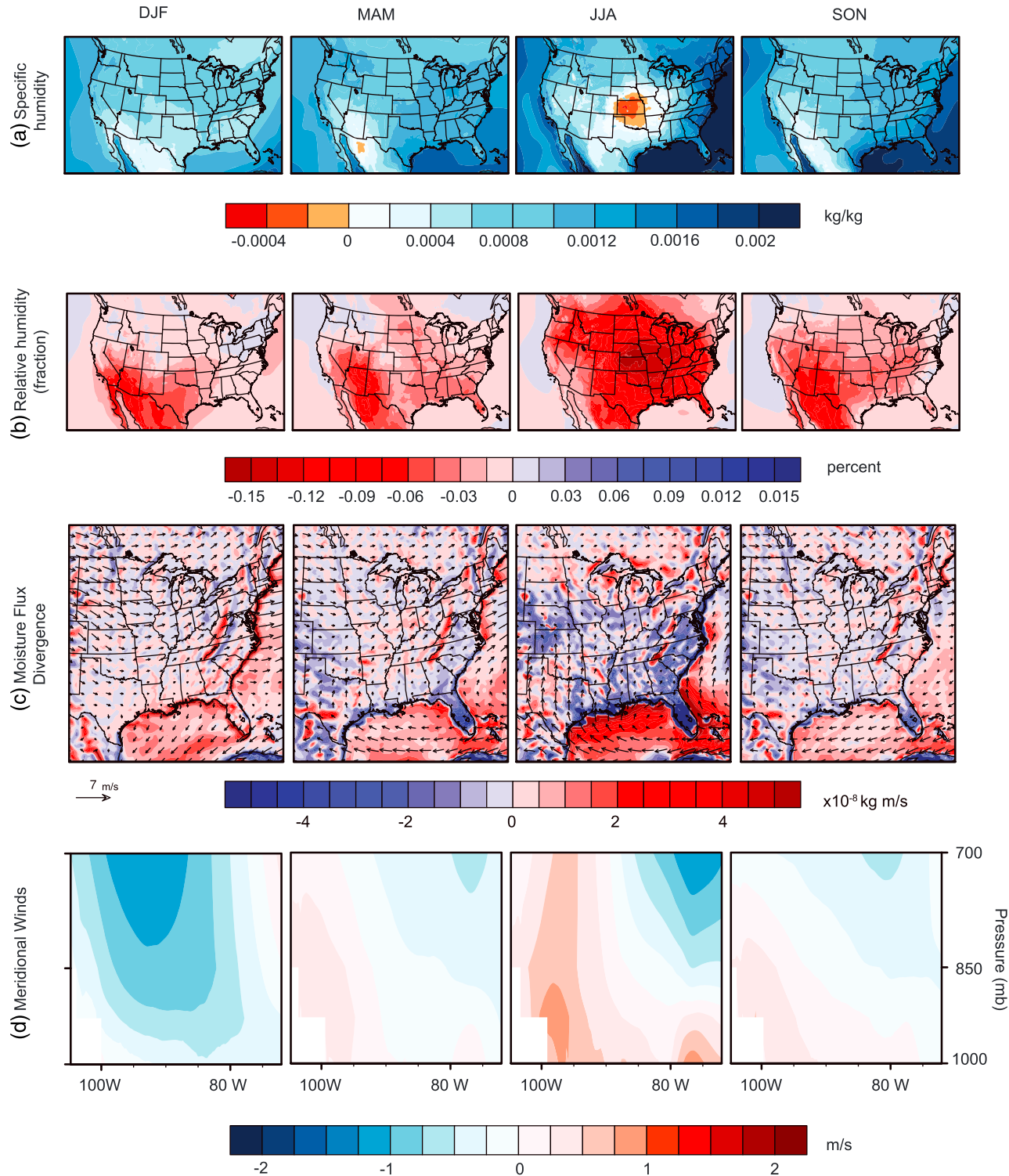


Figure 18. Anomalies in (a) specific humidity, (b) relative humidity, and (c) moisture flux divergence for (105°W – 72°W) at the surface (negative values indicate convergence) and (d) meridional winds averaged across 28°N – 38°N for (105°W – 72°W) domain, in 2070–2099 relative to the baseline (1970–1999) values.

mid-21st century precipitation projections over North America from internal (natural) climate system variability. Their results indicate that substantial natural variability in precipitation leads to uncertainty in the magnitude and direction of precipitation change in large parts of the U.S. Therefore, this five-member ensemble is not sufficient to capture the full scope of internal

climate variability over the near-term decades [Deser *et al.*, 2012]. We also cannot address the uncertainty in projections that arise from inter-model differences in representing physical processes [Hawkins and Sutton, 2009, 2011]. Hawkins and Sutton [2011] suggest that the internal climate system variability is likely to be the dominant source

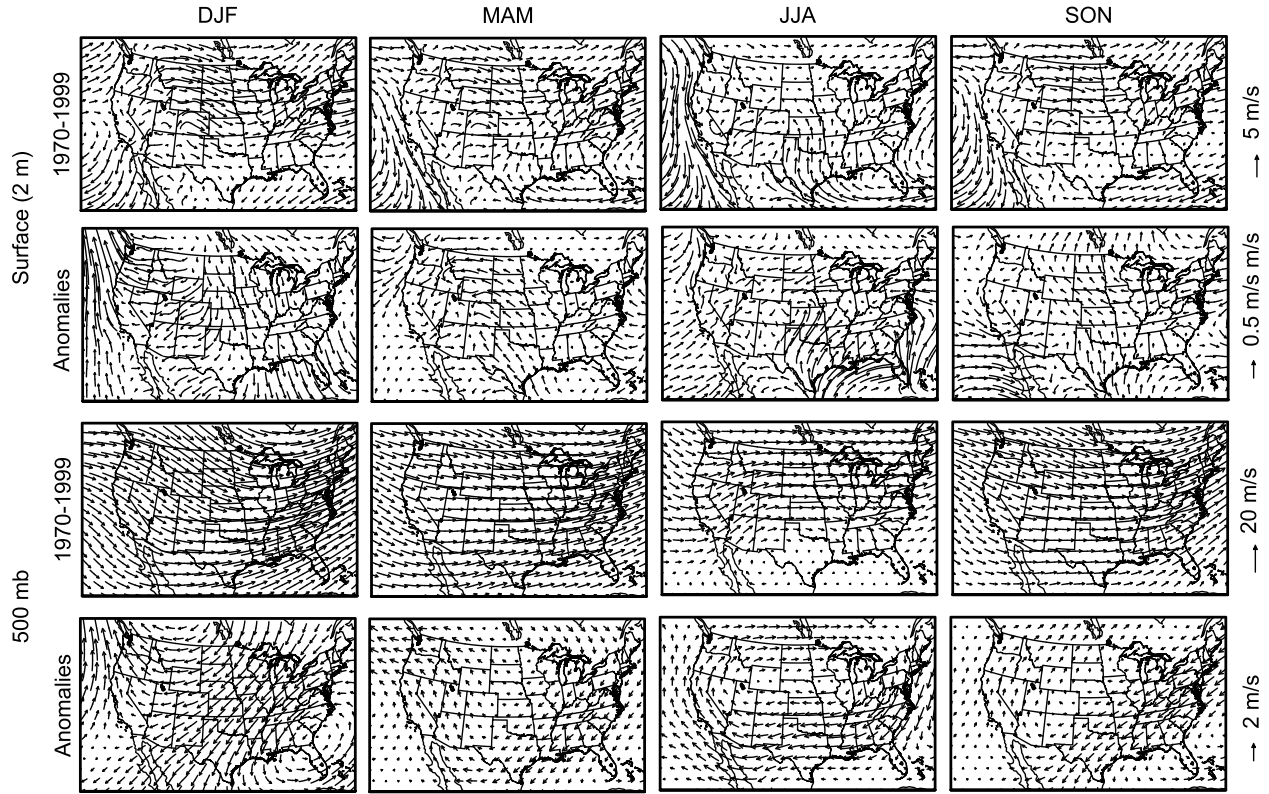


Figure 19. Surface (2 m) and 500 mbar wind vectors in the baseline period (1970–1999) and anomalies in 2070–2099 relative to the baseline values.

of uncertainty in precipitation change in the near term over North America, whereas model uncertainty will dominate in the medium to long term. The subsequent single-model results of *Deser et al.* [2012] suggest greater internal variability than was accessible in the smaller single-model ensembles assessed by *Hawkins and Sutton* [2009, 2011] and thereby suggest that the internal variability uncertainty could be even greater.

[58] We compare these sources of uncertainty by examining the intra-ensemble spread in projections of annual precipitation metrics in the CCSM3-RegCM3 ensemble with inter-model spread in the NARCCAP ensemble (Figure 20). Although the five-member CCSM3-RegCM3 ensemble and the 10-member NARCCAP ensemble do not capture the full range of these uncertainties, we can get some insights into their significance for the current precipitation metrics. We note here that there are considerable known differences in skill of the NARCCAP ensemble members (Figure 2). Further, our comparison is restricted to the mid-century period (2041–2069) due to the limited temporal availability of NARCCAP.

[59] For the mid-century, the intra-ensemble spread in projections of total precipitation, number of dry days, and extreme event intensity is comparable to the inter-model spread in most regions of the U.S. In contrast, the inter-model spread dominates for all other metrics. Additionally, the inter-model spread between simulations of one RCM nested in different AOGCMs is smaller than the spread between different RCMs nested in the same AOGCM. For all the metrics being examined, this result is valid across every region except the Northwest. Furthermore, uncertainty in

the direction of change exists for several of these metrics in both ensembles, although this varies by region. For example, in the Southwest, the ensemble mean change in extreme event frequency is positive in both ensembles. However, several of the NARCCAP models and two of the five CCSM3-RegCM3 ensemble members exhibit negative changes in this metric. Similarly, in all regions except the Southwest, one or both ensembles display an uncertainty in the direction of total precipitation change. This analysis suggests that the relative contribution of internal variability and differences in model response varies by region and depends on the variable of interest.

[60] Further, although we use a nested domain that covers the full contiguous U.S. and is therefore sufficiently large to capture most of the regional features that are likely to influence precipitation, there are important interactions with large-scale atmospheric features that could potentially have been neglected through the one-way nesting approach used here [*Lorenz and Jacob*, 2005]. Likewise, the 25 km hydrostatic resolution is not sufficiently fine to resolve the convective processes that are critical for much of the precipitation that falls over the U.S. (e.g., [*Trapp et al.*, 2007b; *Trapp et al.*, 2011]). The present study also neglects future land-use change that could substantially influence climate [*Feddema et al.*, 2005], including regional atmospheric circulation [*Diffenbaugh*, 2009]. Additionally, the current model configuration excludes the effect of transient changes in aerosols that have the potential to significantly affect the hydrological cycle through their microphysical effects on clouds and direct radiative forcing [*Ramanathan et al.*, 2001].

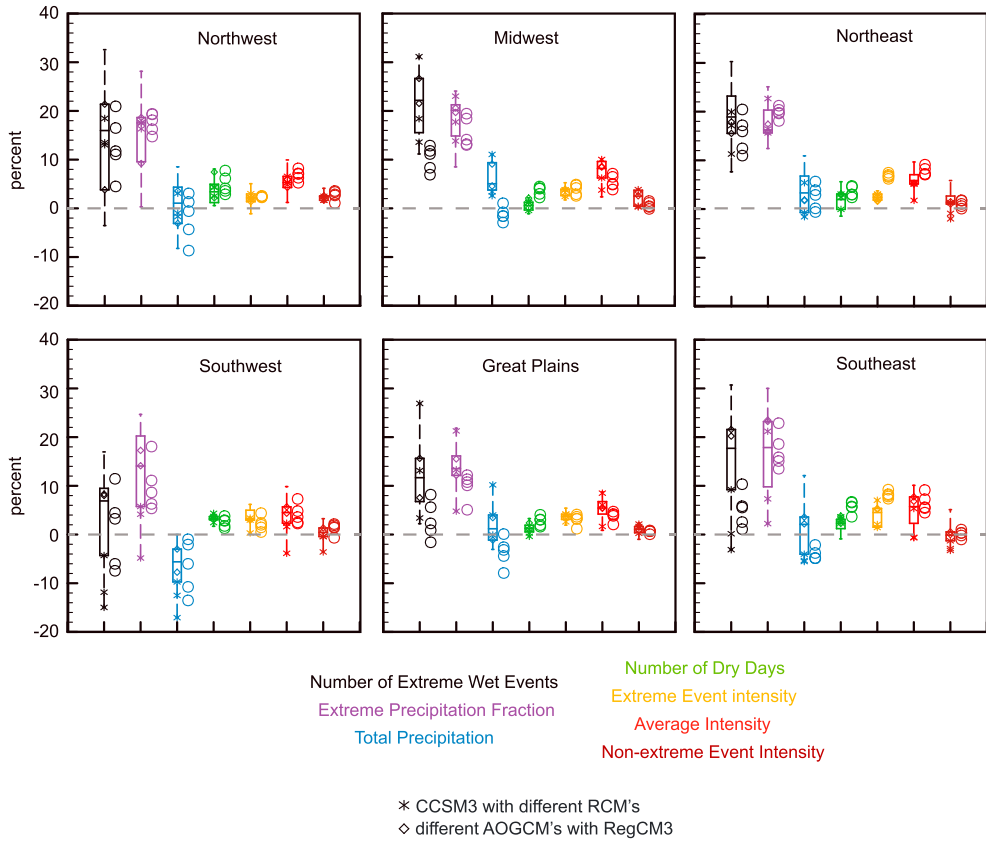


Figure 20. Comparison of changes in precipitation metrics from the five-member CCSM3-RegCM3 ensemble (circles) with the 10-member NARCCAP ensemble (box plots) for the period 2041–2069 relative to 1971–1999. The whiskers of the box plots represent the minimum and maximum, bounds of the box represent 25th and 75th percentiles, and the horizontal line represents median of the percent changes from the NARCCAP models. Colors represent each of the seven precipitation metrics. Stars represent NARCCAP realizations of CCSM3 with different RCMs, and diamonds represent realizations of RegCM3 nested within different GCMs.

[61] Despite these limitations, our transient, multi-member, century-scale high-resolution climate model experiment provides a unique opportunity to probe the transient response of extreme precipitation to global warming. Previous studies show that the high spatial resolution helps to capture the fine-scale processes such as soil-moisture-temperature and soil-moisture-precipitation feedbacks that control the regional response to global warming [Rauscher *et al.*, 2008; Diffenbaugh *et al.*, 2005; Fischer *et al.*, 2007]. Likewise, the multiple realizations and century-scale integration length provide the opportunity to explore the temporal emergence of changes that is important for adaptation and mitigation decisions [Diffenbaugh *et al.*, 2011; Hawkins and Sutton, 2009, 2011; Giorgi and Bi, 2009]. Given the unique nature of our climate model experiment, similar transient, multi-member high-resolution experiments using different climate models are needed in order to corroborate our results.

5. Conclusions

[62] We quantify the response of the frequency, intensity, and duration of wet and dry extremes in the United States to elevated global greenhouse forcing. Our results are consistent with the intensification of the hydrological cycle

predicted from theoretical arguments. The greatest mean precipitation anomalies occur in the northern latitudes in spring (positive) and the central and southern U.S. in summer (negative). We find co-occurring increases in both the frequency of wet extremes and the frequency of dry days, length of dry spells, and intensity of precipitation over most parts of the continental U.S. Anomalies in these metrics occur in every season, with the most widespread increases in wet extremes in spring and dry extremes in summer.

[63] Significant anomalies emerge in the frequencies of wet extremes and average intensities of precipitation events over parts of the U.S. by mid-century that expand and intensify to most of the U.S. in the late 21st century. These changes in precipitation extremes result from changes in atmospheric circulation, atmospheric moisture availability, and daily-scale precipitation variability. Anomalies in extreme precipitation fraction in most regions result from the increasing ratio of extreme wet days to rain days, as the extreme event intensity changes only moderately. In addition, seasonal anomalies in precipitation extremes are evident in some regions that do not show any changes at the annual scale, highlighting the importance of seasonal-scale (and potentially subseasonal-scale) analysis of precipitation extremes.

[64] Substantial increases in the intensity of precipitation events, the frequency of both wet and dry extremes, and the duration of consecutive wet or dry periods have important implications for water availability. For example, the projected widespread drying in the southwestern U.S. in all seasons is likely to significantly impact water resource availability in the region [Cayan *et al.*, 2010]. Likewise, prolonged droughts or extremely heavy precipitation can result in severe crop yield losses [Rosenzweig *et al.*, 2002; Rosenzweig *et al.*, 2001]. Some level of autonomous adaptation has occurred in response to the warming in agricultural [Mechler *et al.*, 2010] and other human systems [Rosenzweig and Wilbanks, 2010]. However, there still is extensive damage from extreme weather events such as floods, hurricanes, droughts, and heat waves across the world. While our results do not directly quantify the influence of such changes on floods and droughts, increasing frequency of extreme precipitation and longer dry periods are more likely to create conditions for such hazards [Kunkel *et al.*, 1999]. Although the present study is focused over the contiguous U.S., the insights gained about the processes regulating local- and regional-scale variations in the extreme precipitation response have relevance for understanding climate change in other regions of the world, particularly given that few high-resolution century-scale ensemble experiments are currently available.

[65] **Acknowledgments.** We thank J.S. Mankin, C.B. Skinner, and D. Swain for helpful discussions and three anonymous reviewers for their insightful comments. We acknowledge the support of Rosen Center for Advanced Computing (RCAC) at Purdue University for providing the computing resources for generating and storing the simulations and the Center for Computational Earth and Environmental Science (CEES) at Stanford University for providing the computing resources for analyzing the simulations. We thank the NCAR Climate Variability and Change Working Group for making the CCSM3 simulations available. We also thank the North American Regional Climate Change Assessment Program (NARCCAP) for providing the data used in this paper. NARCCAP is funded by the National Science Foundation (NSF), the U.S. Department of Energy (DoE), the National Oceanic and Atmospheric Administration (NOAA), and the U.S. Environmental Protection Agency Office of Research and Development (EPA). Our work is supported by NIH Award 1R01AI090159-01 and DOE award DE-SC005171.

References

- Allan, R. P., and B. J. Soden (2008), Atmospheric warming and the amplification of precipitation extremes, *Science*, 321(5895), 1481–1484, doi:10.1126/science.1160787.
- Allen, M. R., and W. J. Ingram (2002), Constraints on future changes in climate and the hydrologic cycle, *Nature*, 419(6903), 224–232.
- Ashfaq, M., Y. Shi, W.-w. Tung, R. J. Trapp, X. Gao, J. S. Pal, and N. S. Diffenbaugh (2009), Suppression of south Asian summer monsoon precipitation in the 21st century, *Geophys. Res. Lett.*, 36, L01704, doi:10.1029/2008GL036500.
- Ashfaq, M., L. C. Bowling, K. Cherkauer, J. S. Pal, and N. S. Diffenbaugh (2010), Influence of climate model biases and daily-scale temperature and precipitation events on hydrological impacts assessment: A case study of the United States, *J. Geophys. Res.*, 115, D14116, doi:10.1029/2009JD012965.
- Ballester, J., X. Rodó, and F. Giorgi (2010), Future changes in Central Europe heat waves expected to mostly follow summer mean warming, *Clim. Dyn.*, 35(7), 1191–1205, doi:10.1007/s00382-009-0641-5.
- Brooks, H. (2003), The spatial distribution of severe thunderstorm and tornado environments from global reanalysis data, *Atmos. Res.*, 67–68, 73–94, doi:10.1016/S0169-8095(03)00045-0.
- Brown, P. J., R. S. Bradley, and F. T. Keimig (2010), Changes in extreme climate indices for the northeastern United States, 1870–2005, *J. Clim.*, 23(24), 6555–6572, doi:10.1175/2010jcli3363.1.
- Burke, E. J., S. J. Brown, and N. Christidis (2006), Modeling the recent evolution of global drought and projections for the twenty-first century with the Hadley Centre Climate Model, *J. Hydrometeorol.*, 7(5), 1113–1125, doi:10.1175/jhm544.1.
- Cayan, D. R., T. Das, D. W. Pierce, T. P. Barnett, M. Tyree, and A. Gershunov (2010), Future dryness in the southwest US and the hydrology of the early 21st century drought, *Proc. Nat. Acad. Sci. U. S. A.*, 107(50), 21,271–21,276, doi:10.1073/pnas.0912391107.
- Chen, P., and M. Newman (1998), Rossby wave propagation and the rapid development of upper-level anomalous anticyclones during the 1988 U. S. drought, *J. Clim.*, 11(10), 2491–2504, doi:10.1175/1520-0442(1998)011<2491:rwpatr>2.0.co;2.
- Christensen, J. H., et al. (2007), Regional climate projections, in *Climate Change 2007: The Physical Science Basis. Contribution of Working Group I to the Fourth Assessment Report of the Intergovernmental Panel on Climate Change*, edited by S. Solomon *et al.*, pp. 848–940, Cambridge Univ. Press, Cambridge, U.K.
- Cook, K. H., E. K. Vizy, Z. S. Launer, and C. M. Patricola (2008), Springtime intensification of the great plains low-level jet and midwest precipitation in GCM simulations of the twenty-first century, *J. Clim.*, 21(23), 6321–6340, doi:10.1175/2008jcli2355.1.
- Davies-Jones, R. (2002), Linear and nonlinear propagation of supercell storms, *J. Atmos. Sci.*, 59(22), 3178–3205, doi:10.1175/1520-0469(2003)059<3178:lanpos>2.0.co;2.
- Deser, C., R. Knutti, S. Solomon, and A. S. Phillips (2012), Communication of the role of natural variability in future North American climate, *Nat. Clim. Change*, 2(11), 775–779, doi:<http://dx.doi.org/10.1038/nclimate1562>.
- Di Luca, A., R. de Elía, and R. Laprise (2012), Potential for added value in precipitation simulated by high-resolution nested Regional Climate Models and observations, *Clim. Dyn.*, 38(5), 1229–1247, doi:10.1007/s00382-011-1068-3.
- Diffenbaugh, N. (2009), Influence of modern land cover on the climate of the United States, *Clim. Dyn.*, 33(7–8), 945–958, doi:10.1007/s00382-009-0566-z.
- Diffenbaugh, N. S., and M. Ashfaq (2007), Response of California Current forcing to mid-Holocene insolation and sea surface temperatures, *Paleoceanography*, 22, PA3101, doi:10.1029/2006PA001382.
- Diffenbaugh, N. S., and M. Ashfaq (2010), Intensification of hot extremes in the United States, *Geophys. Res. Lett.*, 37, L15701, doi:10.1029/2010GL043888.
- Diffenbaugh, N. S., J. S. Pal, R. J. Trapp, and F. Giorgi (2005), Fine-scale processes regulate the response of extreme events to global climate change, *Proc. Nat. Acad. Sci. U.S.A.*, 102(44), 15,774–15,778, doi:10.1073/pnas.0506042102.
- Diffenbaugh, N. S., F. Giorgi, and J. S. Pal (2008), Climate change hotspots in the United States, *Geophys. Res. Lett.*, 35, L16709, doi:10.1029/2008GL035075.
- Diffenbaugh, N. S., M. Ashfaq, and M. Scherer (2011), Transient regional climate change: Analysis of the summer climate response in a high-resolution, century-scale ensemble experiment over the continental United States, *J. Geophys. Res.*, 116, D24111, doi:10.1029/2011JD016458.
- Dominguez, F., E. Rivera, D. P. Lettenmaier, and C. L. Castro (2012), Changes in winter precipitation extremes for the western United States under a warmer climate as simulated by regional climate models, *Geophys. Res. Lett.*, 39, L05803, doi:10.1029/2011GL050762.
- Duffy, P. B., B. Govindasamy, J. P. Lorino, J. Milovich, K. R. Sperber, K. E. Taylor, M. F. Wehner, and S. L. Thompson (2003), High-resolution simulations of global climate, Part 1: Present climate, *Clim. Dyn.*, 21, 371–390, doi:10.1007/s00382-003-0339-z.
- Easterling, D. R. (2000), Climate extremes: Observations, modeling, and impacts, *Science*, 289(5487), 2068–2074, doi:10.1126/science.289.5487.2068.
- Emori, S., and S. J. Brown (2005), Dynamic and thermodynamic changes in mean and extreme precipitation under changed climate, *Geophys. Res. Lett.*, 32(17), L17706, doi:10.1029/2005GL023272.
- Feddema, J. J., K. W. Oleson, G. B. Bonan, L. O. Mearns, L. E. Buja, G. A. Meehl, and W. M. Washington (2005), The importance of land-cover change in simulating future climates, *Science*, 310(5754), 1674–1678, doi:10.1126/science.1118160.
- Field, C. B., et al. (Eds.) (2012) Summary for policymakers, in: *Managing the Risks of Extreme Events and Disasters to Advance Climate Change Adaptation. A Special Report of Working Groups I and II of the Intergovernmental Panel on Climate Change*, pp. 1–19, Cambridge Univ. Press, Cambridge, U.K.
- Fischer, E. M., S. I. Seneviratne, P. L. Vidale, D. Lüthi, and C. Schär (2007), Soil moisture–atmosphere interactions during the 2003 European summer heat wave, *J. Clim.*, 20(20), 5081–5099, doi:10.1175/jcli4288.1.
- Frich, P., L. V. Alexander, P. Della-Marta, B. Gleason, M. Haylock, A. Klein Tank, and T. C. Peterson (2002), Global changes in climatic extremes during the 2nd half of the 20th century, *Clim. Res.*, 19, 193–212.
- Gao, X., and F. Giorgi (2008), Increased aridity in the Mediterranean region under greenhouse gas forcing estimated from high resolution simulations

- with a regional climate model, *Global Planet. Change*, 62(3–4), 195–209, doi:10.1016/j.gloplacha.2008.02.002.
- Giorgi, F., and X. Bi (2009), Time of emergence (TOE) of GHG-forced precipitation change hot-spots, *Geophys. Res. Lett.*, 36, L06709, doi:10.1029/2009GL037593.
- Giorgi, F., E. S. Im, E. Coppola, N. S. Diffenbaugh, X. J. Gao, L. Mariotti, and Y. Shi (2011), Higher hydroclimatic intensity with global warming, *J. Clim.*, 24(20), 5309–5324, doi:10.1175/2011jcli3979.1.
- Gleason, K. L., J. H. Lawrimore, D. H. Levinson, T. R. Karl, and D. J. Karoly (2008), A revised U.S. climate extremes index, *J. Clim.*, 21(10), 2124–2137, doi:10.1175/2007jcli1883.1.
- Gutowski, W. J., et al. (2010), Regional extreme monthly precipitation simulated by NARCCAP RCMs, *J. Hydrometeorol.*, 11(6), 1373–1379, doi:10.1175/2010jhm1297.1.
- Hall, N. M. J., B. J. Hoskins, P. J. Valdes, and C. A. Senior (1994), Storm tracks in a high-resolution GCM with doubled carbon dioxide, *Q. J. R. Meteorol. Soc.*, 120(519), 1209–1230, doi:10.1002/qj.49712051905.
- Hawkins, E., and R. Sutton (2009), The potential to narrow uncertainty in regional climate predictions, *Bull. Am. Meteorol. Soc.*, 90(8), 1095–1107, doi:10.1175/2009bams2607.1.
- Hawkins, E., and R. Sutton (2011), The potential to narrow uncertainty in projections of regional precipitation change, *Clim. Dyn.*, 37(1), 407–418, doi:10.1007/s00382-010-0810-6.
- Held, I. M., and B. J. Soden (2006), Robust responses of the hydrological cycle to global warming, *J. Clim.*, 19(21), 5686–5699, doi:10.1175/jcli3990.1.
- Higgins, R. W., W. Shi, E. Yarosh, and R. Joyce (2000), Improved U.S. precipitation quality control system and analysis, Natl. Cent. for Environ. Predict., Clim. Predict. Cent., Camp Springs, Md.
- Hong, S.-Y., and E. Kalnay (2002), The 1998 Oklahoma–Texas drought: Mechanistic experiments with NCEP global and regional models, *J. Clim.*, 15(9), 945–963, doi:10.1175/1520-0442(2002)015<0945:tdtme>2.0.co;2.
- Hu, Q., and S. Feng (2010), Influence of the Arctic oscillation on central United States summer rainfall, *J. Geophys. Res.*, 115, D01102, doi:10.1029/2009JD011805.
- Kanamitsu, M., W. Ebisuzaki, J. Woollen, S.-K. Yang, J. J. Hnilo, M. Fiorino, and G. L. Potter (2002), NCEP–DOE AMIP-II Reanalysis (R-2), *Bull. Am. Meteorol. Soc.*, 83(11), 1631–1643, doi:10.1175/bams-83-11-1631.
- Katz, R. W., and B. G. Brown (1992), Extreme events in a changing climate: Variability is more important than averages, *Clim. Change*, 21(3), 289–302, doi:10.1007/bf00139728.
- Kunkel, K. E., K. Andsager, D. R. Easterling (1999), Long-term trends in extreme precipitation events over the conterminous United States and Canada, *J. Clim.*, 12(8), 2515–2527, doi:10.1175/1520-0442(1999)012<2515:lttiep>2.0.co;2.
- Lau, W. K. M., H. T. Wu, and K. M. Kim (2013), A canonical response of precipitation characteristics to global warming from CMIP5 models, *Geophys. Res. Lett.*, doi:10.1002/grl.50420, in press.
- Lintner, B., M. Biasutti, N. S. Diffenbaugh, J.-E. Lee, M. J. Niznik, and K. L. Findell (2012), Amplification of wet and dry month occurrence over tropical land regions in response to global warming, *J. Geophys. Res.*, 117, D11106, doi:10.1029/2012JD017499.
- Lionello, P., and F. Giorgi (2007), Winter precipitation and cyclones in the Mediterranean region: Future climate scenarios in a regional simulation, *Adv. Geosci.*, 12, 153–158, doi:10.5194/adgeo-12-153-2007.
- Lorenz, P., and D. Jacob (2005), Influence of regional scale information on the global circulation: A two-way nesting climate simulation, *Geophys. Res. Lett.*, 32, L18706, doi:10.1029/2005GL023351.
- Lott, N., A. Smith, T. Houston, K. Shein, and J. Crouch (2012), *Billion dollar U.S. weather/climate disasters, 1980–2011*, Natl. Clim. Data Cent., Asheville, N. C.
- Manabe, S., and R. T. Wetherald (1987), Large-scale changes of soil wetness induced by an increase in atmospheric carbon dioxide, *J. Atmos. Sci.*, 44(8), 1211–1236, doi:10.1175/1520-0469(1987)044<1211:lscosw>2.0.co;2.
- Mearns, L. O., W. Gutowski, R. Jones, R. Leung, S. McGinnis, A. Nunes, and Y. Qian (2009), A regional climate change assessment program for North America, *Eos. Trans. AGU*, 90(36), 311–311, doi:10.1029/2009EO360002.
- Mearns, L. O., et al. (2007), updated 2012. *The North American Regional Climate Change Assessment Program dataset*, National Center for Atmospheric Research Earth System Grid data portal, Boulder, CO. Data downloaded 2013-06-21, [doi:10.5065/D6RN35ST].
- Mearns, L. O., et al. (2012), The North American Regional Climate Change Assessment Program: Overview of phase I results, *Bull. Am. Meteorol. Soc.*, 93(9), 1337–1362, doi:10.1175/bams-d-11-00223.1.
- Mechler, R., S. Hochrainer, A. Aaheim, H. Salen, and A. Wreford (2010), Modelling economic impacts and adaptation to extreme events: Insights from European case studies, *Mitig. Adapt. Strat. Glob. Change*, 15(7), 737–762, doi:10.1007/s11027-010-9249-7.
- Meehl, G. A., J. M. Arblaster, and C. Tebaldi (2005), Understanding future patterns of increased precipitation intensity in climate model simulations, *Geophys. Res. Lett.*, 32, L18719, doi:10.1029/2005GL023680.
- Meehl, G. A., W. M. Washington, B. D. Santer, W. D. Collins, J. M. Arblaster, A. Hu, D. M. Lawrence, H. Teng, L. E. Buja, and W. G. Strand (2006), Climate change projections for the twenty-first century and climate change commitment in the CCSM3, *J. Clim.*, 19(11), 2597–2616, doi:10.1175/jcli3746.1.
- Meehl, G., C. Covey, K. Taylor, T. Delworth, R. B. M. Stouffer, M. Latif, B. McAvaney, and J. Mitchell (2007), The WCRP CMIP3 multimodel dataset: A new era in climate change research, *Bull. Am. Meteorol. Soc.*, 88(9), 1383–1394, doi:10.1175/bams-88-9-1383.
- Mishra, V., and D. P. Lettenmaier (2011), Climatic trends in major U.S. urban areas, 1950–2009, *Geophys. Res. Lett.*, 38, L16401, doi:10.1029/2011GL048255.
- Nackenovic, N., et al. (2000), Special Report on Emissions Scenarios, Cambridge Univ. Press, 599 pp., Cambridge, U. K.
- National Assessment Synthesis Team (NAST) (2000), Climate change impacts on the United States: *The potential consequences of climate variability and change*, U.S. Global Change R. Program, Washington, D. C.
- NOAA (2011), State of the climate: National overview for Annual 2011, National Climate Data Center, Asheville, N.C.
- NOAA (2012a), State of the climate: Drought for February 2012, Natl. Clim. Data Cent., Asheville, N. C.
- NOAA (2012b), State of the climate: Drought for August 2012, Natl. Clim. Data Cent., Asheville, N. C.
- Noake, K., D. Polson, G. Hegerl, and X. Zhang (2012), Changes in seasonal land precipitation during the latter twentieth-century, *Geophys. Res. Lett.*, 39, L03706, doi:10.1029/2011GL050405.
- O’Gorman, P. A., and T. Schneider (2009), The physical basis for increases in precipitation extremes in simulations of 21st-century climate change, *Proc. Natl. Acad. Sci. U. S. A.*, 106(35), 14,773–14,777, doi:10.1073/pnas.0907610106.
- Pal, J. S., et al. (2007), Regional climate modeling for the developing world: The ICTP RegCM3 and RegCNET, *Bull. Am. Meteorol. Soc.*, 88(9), 1395–1409.
- Peterson, T. C., X. Zhang, M. Brunet-India, and J. L. Vázquez-Aguirre (2008), Changes in North American extremes derived from daily weather data, *J. Geophys. Res.*, 113, D07113, doi:10.1029/2007JD009453.
- Pryor, S. C., and R. J. Barthelmie (2011), Assessing climate change impacts on the near-term stability of the wind energy resource over the United States, *Proc. Natl. Acad. Sci. U. S. A.*, 108(20), 8167–8171, doi:10.1073/pnas.1019388108.
- Pryor, S. C., J. A. Howe, and K. E. Kunkel (2009), How spatially coherent and statistically robust are temporal changes in extreme precipitation in the contiguous USA?, *Int. J. Climatol.*, 29(1), 31–45, doi:10.1002/joc.1696.
- Ramanathan, V., P. J. Crutzen, J. T. Kiehl, and D. Rosenfeld (2001), Aerosols, climate, and the hydrological cycle, *Science*, 294(5549), 2119–2124, doi:10.1126/science.1064034.
- Rasmussen, D. J., T. Holloway, and G. F. Nemet (2011), Opportunities and challenges in assessing climate change impacts on wind energy—A critical comparison of wind speed projections in California, *Environ. Res. Lett.*, 6(2), 024008.
- Rauscher, S. A., J. S. Pal, N. S. Diffenbaugh, and M. M. Benedetti (2008), Future changes in snowmelt-driven runoff timing over the western US, *Geophys. Res. Lett.*, 35, L16703, doi:10.1029/2008GL034424.
- Rosenzweig, C., and T. J. Wilbanks (2010), The state of climate change vulnerability, impacts, and adaptation research: Strengthening knowledge base and community, *Clim. Change*, 100(1), 103–106, doi:10.1007/s10584-010-9826-5.
- Rosenzweig, C., A. Iglesias, X. B. Yang, P. R. Epstein, and E. Chivian (2001), Climate change and extreme weather events: implications for food production, plant diseases, and pests, *Global Change Human Health*, 2(2), 90–104, doi:10.1023/a:1015086831467.
- Rosenzweig, C., F. N. Tubiello, R. Goldberg, E. Mills, and J. Bloomfield (2002), Increased crop damage in the US from excess precipitation under climate change, *Global Environ. Change*, 12(3), 197–202, doi:10.1016/s0959-3780(02)00008-0.
- Russo, S., and A. Sterl (2012), Global changes in seasonal means and extremes of precipitation from daily climate model data, *J. Geophys. Res.*, 117, D01108, doi:10.1029/2011JD016260.
- Salinger, M. J., and G. M. Griffiths (2001), Trends in New Zealand daily temperature and rainfall extremes, *Int. J. Climatol.*, 21(12), 1437–1452.
- Santer, B. D., et al. (2007), Identification of human-induced changes in atmospheric moisture content, *Proc. Natl. Acad. Sci.*, 104(39), 15,248–15,253, doi:10.1073/pnas.0702872104.

- Seager, R., et al. (2007), Model projections of an imminent transition to a more arid climate in southwestern North America, *Science*, **316**(5828), 1181–1184, doi:10.1126/science.1139601.
- Seth, A., S. Rauscher, S. Camargo, J.-H. Qian, and J. Pal (2007), RegCM3 regional climatologies for South America using reanalysis and ECHAM global model driving fields, *Clim. Dyn.*, **28**(5), 461–480, doi:10.1007/s00382-006-0191-z.
- Tebaldi, C., K. Hayhoe, J. M. Arblaster, and G. A. Meehl (2006), Going to the extremes, *Clim. Change*, **79**(3–4), 185–211, doi:10.1007/s10584-006-9051-4.
- Trapp, R. J., N. S. Diffenbaugh, H. E. Brooks, M. E. Baldwin, E. D. Robinson, and J. S. Pal (2007a), Changes in severe thunderstorm environment frequency during the 21st century caused by anthropogenically enhanced global radiative forcing, *Proc. Natl. Acad. Sci. U. S. A.*, **104**(50), 19,719–19,723, doi:10.1073/pnas.0705494104.
- Trapp, R. J., B. A. Halvorson, and N. S. Diffenbaugh (2007b), Telescoping, multimodel approaches to evaluate extreme convective weather under future climates, *J. Geophys. Res.*, **112**, D20109, doi:10.1029/2006JD008345.
- Trapp, R. J., N. S. Diffenbaugh, and A. Gluhovsky (2009), Transient response of severe thunderstorm forcing to elevated greenhouse gas concentrations, *Geophys. Res. Lett.*, **36**, L01703, doi:10.1029/2008GL036203.
- Trapp, R., E. Robinson, M. Baldwin, N. Diffenbaugh, and B. J. Schwedler (2011), Regional climate of hazardous convective weather through high-resolution dynamical downscaling, *Clim. Dyn.*, **37**(3–4), 677–688, doi:10.1007/s00382-010-0826-y.
- Trenberth, K. E. (1999), Conceptual framework for changes of extremes of the hydrological cycle with climate change, *Clim. Change*, **42**(1), 327–339, doi:10.1023/a:1005488920935.
- Trenberth, K. E., and C. J. Guillemot (1996), Physical processes involved in the 1988 drought and 1993 floods in North America, *J. Clim.*, **9**(6), 1288–1298, doi:10.1175/1520-0442(1996)009<1288:ppiitd>2.0.co;2.
- Trenberth, K. E., A. Dai, R. M. Rasmussen, and D. B. Parsons (2003), The changing character of precipitation, *Bull. Am. Meteorol. Soc.*, **84**(9), 1205–1217, doi:10.1175/bams-84-9-1205.
- Tuttle, J. D., and C. A. Davis (2006), Corridors of warm season precipitation in the central United States, *Mon. Weather Rev.*, **134**(9), 2297–2317, doi:10.1175/mwr3188.1.
- Walker, M. D., and N. S. Diffenbaugh (2009), Evaluation of high-resolution simulations of daily-scale temperature and precipitation over the United States, *Clim. Dyn.*, **33**(7–8), 1131–1147, doi:10.1007/s00382-009-0603-y.
- Wang, S.-Y., R. R. Gillies, E. S. Takle, and W. J. Gutowski Jr. (2009), Evaluation of precipitation in the Intermountain Region as simulated by the NARCCAP regional climate models, *Geophys. Res. Lett.*, **36**, L11704, doi:10.1029/2009GL037930.
- Wehner, M. F. (2004), Predicted twenty-first-century changes in seasonal extreme precipitation events in the parallel climate model, *J. Clim.*, **17**(21), 4281–4290, doi:10.1175/jcli3197.1.
- Wehner, M. (2013), Very extreme seasonal precipitation in the NARCCAP ensemble: Model performance and projections, *Clim. Dyn.*, **40**(1–2), 59–80, doi:10.1007/s00382-012-1393-1.
- Weisman, M. L., and J. B. Klemp (1982), The dependence of numerically simulated convective storms on vertical wind shear and buoyancy, *Mon. Weather Rev.*, **110**(6), 504–520, doi:10.1175/1520-0493(1982)110<0504:tdonsc>2.0.co;2.
- Wentz, F. J., L. Ricciardulli, K. Hilburn, and C. Mears (2007), How much more rain will global warming bring?, *Science*, **317**(5835), 233–235, doi:10.1126/science.1140746.
- Wetherald, R. T., and S. Manabe (1995), The mechanisms of summer dryness induced by greenhouse warming, *J. Clim.*, **8**(12), 3096–3108, doi:10.1175/1520-0442(1995)008<3096:tmosdi>2.0.co;2.
- Yin, J. H. (2005), A consistent poleward shift of the storm tracks in simulations of 21st century climate, *Geophys. Res. Lett.*, **32**, L18701, doi:10.1029/2005GL023684.
- Zhang, X., F. W. Zwiers, G. C. Hegerl, F. H. Lambert, N. P. Gillett, S. Solomon, P. A. Stott, and T. Nozawa (2007), Detection of human influence on twentieth-century precipitation trends, *Nature*, **448**(7152), 461–465, doi:10.1038/nature06025.